



# CHORUS

This is the accepted manuscript made available via CHORUS. The article has been published as:

## Correlating structural distributions in silica glass with two-dimensional J-resolved spectroscopy

Deepansh J. Srivastava, Jay H. Baltisberger, Pierre Florian, Franck Fayon, Roman A. Shakhovoy, Michaël Deschamps, Najim Sadiki, and Philip J. Grandinetti

Phys. Rev. B **98**, 134202 — Published 8 October 2018

DOI: [10.1103/PhysRevB.98.134202](https://doi.org/10.1103/PhysRevB.98.134202)

# Correlating Structural Distributions in Silica Glass with 2D *J*-Resolved Spectroscopy

Deepansh J. Srivastava and Philip J. Grandinetti<sup>a</sup>

*Department of Chemistry, Ohio State University,  
100 West 18th Avenue, Columbus, OH 43210, USA*

Jay H. Baltisberger

*Division of Natural Science, Mathematics, and Nursing,  
Berea College, Berea, Kentucky 40403, USA*

Pierre Florian, Franck Fayon, Roman A. Shakhovoy, and Michaël Deschamps

*CNRS, UPR3079 CEMHTI, 1D Avenue de la  
Recherche Scientifique, 45071 Orléans Cedex 2, France*

Najim Sadiki

*PROMES, CNRS, Rambla de la Thermodynamique,  
Tecnosud, 66100 Perpignan, France*

---

<sup>a</sup> Corresponding Author

## Abstract

A 2D  $J$ -resolved magic-angle spinning Nuclear Magnetic Resonance (NMR) spectrum of silica glass at  $^{29}\text{Si}$  natural abundance levels, 4.7%, was measured using the Shifted-Echo Phase Incremented Echo Train Acquisition (SE-PIETA) pulse sequence. At  $^{29}\text{Si}$  natural abundance levels the  $J_{\text{Si-O-Si}}$  couplings splittings appear as overlapping doublet patterns arising from isolated  $^{29}\text{Si-O-}^{29}\text{Si}$  linkages. The experimental 2D  $J$ -resolved spectrum is analyzed to obtain a bi-variate probability distribution correlating the central Si-O-Si angle of a  $\text{Q}^4\text{-Q}^4$  linkage to its mean Si-O-Si angle (seven angles) using relationships between  $^{29}\text{Si}$  isotropic chemical shifts and geminal  $J_{\text{Si-O-Si}}$  coupling of a  $\text{Q}^4\text{-Q}^4$  to its local structure. To obtain a self-consistent bi-variate probability distribution it was necessary to introduce an additional dependence of the  $^{29}\text{Si}$  chemical shift of a  $\text{Q}^4$  on mean Si-O distance as well as mean Si-O-Si angle. The implication of this necessary modification is a positive correlation between Si-O-Si angle and Si-O distance in the silica glass, consistent with recent  $^{17}\text{O}$  NMR measurements on ambient and densified silica glasses but running opposite to the trend generally found in crystalline silica polymorphs. From the analysis of the  $^{29}\text{Si}$  2D  $J$ -resolved spectrum we determine a Si-O-Si bond angle distribution in silica glass as having a mean at  $147.8^\circ$ , a mode at  $147^\circ$  and a standard deviation of  $10.7^\circ$ . Our statistical model for analyzing the experimental  $^{29}\text{Si}$  2D  $J$ -resolved spectrum also indicates that the individual Si-O-Si bond angle distributions are relatively uncorrelated.

## I. INTRODUCTION

Glass structure is a difficult thing to characterize. Any structural model of glass is necessarily statistical in nature, that is, the individual atomic positions cannot be known. When constructing structural models of glasses the most commonly used prior information comes from the static structure factors obtained from diffraction measurements<sup>1,2</sup>, whose Fourier transform is the pair (2-body) correlation function of the material. Unfortunately, in the case of a glass this one-dimensional statistical distribution is smooth and provides few structural constraints<sup>3</sup>. While techniques like Reverse Monte Carlo<sup>4</sup> and recent variants<sup>5,6</sup> rely solely on experimental information, the unfortunate truth is that the information content of most experimental measurements on glass structure is low. Recently devised hybrid methods attempt to incorporate additional prior information from classical and ab initio potentials. The challenges with this approach, however, is in finding accurate potentials that are transferable to structural studies of glasses when they are trained on crystalline databases<sup>3,7</sup>.

Here we focus on the experimental side of the problem by attempting to increase the information content of measurements through the use of more sophisticated multi-dimensional nuclear magnetic resonance (NMR) spectroscopy measurements and spectral analysis. We illustrate this approach in the case of the archetypical network-forming glass, vitreous SiO<sub>2</sub>. In the majority of NMR studies of network forming glasses, where spectra contain a number of resolved “resonances,” spectroscopists focus almost entirely on using NMR spectra to identify and quantify populations of polyhedral units, and polyhedral linkages<sup>8</sup>. This coarse-grain analysis has generated tremendous insight into the structure of glass over the last 30 years, yet it falls short in exploring the full range of noteworthy structural distributions. By using the term “coarse-grain analysis” and referring to “resonances” in quotes, we are highlighting the fact that these resolved “resonances” are inhomogeneously broadened, that is, inside each “resonance” is a mix of homogeneous resonances from numerous structurally distinct sites. The shape of these inhomogeneous “resonances” contains a wealth of structural information, and it is two mappings: (1) from NMR line shape to probability distribution of NMR parameters, and (2) from NMR parameters distribution to probability distribution of structure parameters that lie at the heart of more refined structural assignments of glass NMR spectra. We refer to such a quantitative spectral analysis that produces a probability

distribution for glass structure parameters as a “fine-grain” analysis,

One of the first attempts to perform a fine-grain analysis of an inhomogeneous NMR line shape from a glass was in 1984 by Dupree and Pettifer<sup>9</sup> on the <sup>29</sup>Si magic-angle spinning (MAS) spectrum of silica glass. Using then-recently established correlations between <sup>29</sup>Si isotropic chemical shift and the mean Si-O-Si angle of a tetrahedron, Dupree and Pettifer inverted the MAS line shape of a Q<sup>4</sup> resonance into the Si-O-Si angle distribution of silica. While a direct inversion of the <sup>29</sup>Si MAS spectrum of silica glass yields the distribution of mean Si-O-Si angles of the Q<sup>4</sup> sites, the individual Si-O-Si bond-angle distribution can be obtained in a more sophisticated analysis with the assumption that the four Si-O-Si angles on each Q<sup>4</sup> are statistically independent<sup>9-11</sup>. Unfortunately, in more compositionally diverse silicate glasses the correlation between <sup>29</sup>Si isotropic chemical shift and the mean Si-O-Si angle becomes strongly influenced by the identity of the next nearest neighbor polyhedral units and modifier cations, and the line shape inversion is no longer as simple. These caveats aside, the Dupree and Pettifer study pointed the way towards more systematic inversions of glass spectra.

While NMR spectroscopy of glasses generally suffers the same malady of overlapping resonances as other spectroscopies, NMR has a distinct advantage of not being limited to one spectroscopic dimension. In 1992 Farnan et al<sup>12</sup> used dynamic-angle spinning<sup>13-16</sup> (DAS) NMR to measure the isotropic <sup>17</sup>O NMR line shape of the bridging oxygen in a potassium tetrasilicate glass. Although there is no simple mapping between the <sup>17</sup>O isotropic shift and Si-O-Si angle, they showed that the correlated anisotropic line shapes from the full 2D DAS spectrum can be used to extract mean quadrupolar coupling parameters for each correlated part of the inhomogeneous isotropic line shape. The quadrupolar asymmetry parameter, for which correlations to Si-O-Si angle were known, was then used to invert the isotropic line shape into the mean Si-O-Si angle distribution of the potassium tetrasilicate glass.

Since the work of Farnan et al<sup>12</sup> considerable progress has been made in determining more precise relationships between the <sup>17</sup>O nuclear quadrupolar coupling parameters of the inter-tetrahedral bridging oxygen and its first coordination sphere structure<sup>17-27</sup>. A particular advantage of <sup>17</sup>O 2D DAS is that it can now determine the bivariate distribution of Si-O distances and Si-O-Si angles. In the case of silica this advance was significant because it revealed a strong positive correlation, i.e., Si-O distance increasing with increasing Si-O-Si angle<sup>28,29</sup>. This correlation runs counter to conventional wisdom of a negative corre-

lation in silicate glass structure. Further evidence of this positive correlation could impact our understanding of the role of configuration entropy in stabilizing certain silicate glass structures<sup>30</sup>.

In this work we develop a new approach for determining the bi-variate probability distribution correlating the central Si-O-Si angle of a Q<sup>4</sup>-Q<sup>4</sup> linkage to its mean Si-O-Si angle (seven angles) using relationships between <sup>29</sup>Si isotropic chemical shifts and geminal  $J_{\text{Si-O-Si}}$  coupling of a Q<sup>4</sup>-Q<sup>4</sup> to its local structure. While  $J$  couplings are a powerful probe of structure in liquid-state NMR spectroscopy, they have seen limited use in solid-state NMR studies. This is because (1) the  $J$ -splittings are often tiny compared to line widths in solid-state magic-angle spinning (MAS) NMR and, therefore, difficult to detect, and (2) our understanding of the relationships between  $J$  couplings and local structure had lagged behind other NMR probes of structure, such as chemical shifts and nuclear quadrupole couplings. An important advance in solving the first problem occurred in 2012 with the development of a new NMR method called Phase-Incremented Echo Train Acquisition (PIETA), which not only removes the inhomogeneous broadenings obscuring  $J$  splittings in MAS spectra but also is a method for rapid and sensitive measurement of a 2D  $J$ -resolved spectrum<sup>31</sup>. More recently, Srivastava et al.<sup>32</sup> have addressed the second problem in discovering a robust relationship for converting a geminal  $^2J_{\text{Si-O-Si}}$  coupling into an inter-tetrahedral Si-O-Si angle.

In a previous attempt by Florian et al.<sup>33</sup> in 2009,  $J$ -resolved spectra of <sup>29</sup>Si enriched crystalline and glassy CaSiO<sub>3</sub> were measured. Due to <sup>29</sup>Si enrichment, the spectrum resulted in  $J$  multiplets (Q<sup>2</sup>) for crystalline wollastonite whereas the  $J$ -multiplets rendered the  $J$ -resolved spectrum featureless in CaSiO<sub>3</sub> glass. The number of resonances in a  $J$ -multiplet increase as  $2^n$  with  $n$  neighboring <sup>29</sup>Si. Thus, the degree of complexity introduced to the spectrum by the  $J$  multiplets increases with Q<sup>1</sup> < Q<sup>2</sup> < Q<sup>3</sup> < Q<sup>4</sup>. Since silica glass is entirely Q<sup>4</sup>, 100% <sup>29</sup>Si enrichment gives the worst-case scenario. To make the spectra analysis more tractable we take on the experimentally challenge of measuring the 2D  $J$ -resolved spectrum in silica glass at <sup>29</sup>Si natural abundance levels, 4.7%, where, instead of the overlapping multiplet patterns<sup>33</sup> in <sup>29</sup>Si enriched samples, the  $J$  splittings appear as simpler overlapping doublet patterns arising from isolated <sup>29</sup>Si-O-<sup>29</sup>Si linkages. Another advantage of natural abundance is that the homonuclear dipolar coupling between <sup>29</sup>Si is easily removed with MAS due to its inhomogeneous nature<sup>34</sup>. Most importantly, we develop

and present a detailed spectral analysis for mapping the 2D  $J$ -resolved spectrum into the bi-variate probability distribution correlating the central Si-O-Si angle of a Q<sup>4</sup>-Q<sup>4</sup> linkage to its mean Si-O-Si angle (seven angles) in silica glass which is significantly more information rich than the one dimensional Si-O-Si angle distribution.

## II. THEORETICAL BACKGROUND

### A. $J$ -coupling under echo train acquisition

A theoretical treatment of the detection of homonuclear  $J$ -coupling between spin 1/2 nuclei using echo train acquisition in the context of liquid state NMR<sup>35,36</sup> has been given by Allerhand<sup>35</sup>. For two spin-1/2 nuclei coupled through the  $J$  interaction, the modulation of the  $n^{\text{th}}$  echo predominantly follows

$$s(n) \propto \cos \left[ \pi J n 2\tau - n \sin^{-1} \left\{ \frac{J \sin(\pi R 2\tau)}{R} \right\} \right], \quad (1)$$

where

$$R = (\Delta\nu^2 + J^2)^{1/2}. \quad (2)$$

Here  $2\tau$  is the inter-echo period and  $\Delta\nu$  is the difference in the chemical shifts of the  $J$ -coupled spins. From Eq. (1) one finds the well known behavior that the echo modulation frequency disappears as the strong coupling limit, where  $J \gg \Delta\nu$ , is approached,

$$\lim_{R \rightarrow J} s(n) \rightarrow 1. \quad (3)$$

All resonances close to the strong coupling limit exhibit modulation frequencies of or near 0 Hz.

From Eq. (1) one can also find in the weak coupling limit, where  $J \ll \Delta\nu$ , that

$$s(n) \propto \cos [\pi J n 2\tau (1 - \text{sinc}(\pi R 2\tau))]. \quad (4)$$

It is critical to be aware of two limiting behaviors for echo train acquisition in the weak coupling limit. When  $2\tau$  is large, or more specifically,  $\text{sinc}(\pi R 2\tau) \ll 1$ , this expression simplifies to the expected behavior,

$$\lim_{2\tau \rightarrow \infty} s(n) \rightarrow \cos(\pi J n 2\tau). \quad (5)$$

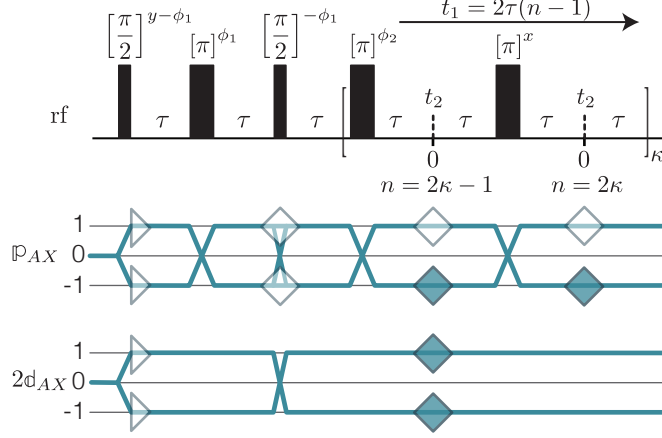


FIG. 1. Graphical representation of the shifted-echo PIETA sequence and relevant symmetry pathways. Here  $\kappa = 1..N$  and  $n = 1..2N$  is echo counter where  $2N$  is the number of echoes acquired.

On the other hand, in the limit that  $2\tau$  goes to zero, i.e.,  $\text{sinc}(\pi R 2\tau) = 1$  the echo modulation frequency disappears,

$$\lim_{2\tau \rightarrow 0} s(n) \rightarrow 1. \quad (6)$$

Thus, even in the weak coupling limit, the  $J$  modulation during echo train acquisition deviates from the expected behavior of Eq. (5), instead giving, according to Eq. (4), a  $\tau$  dependent echo modulation frequency (sinc function variation of the  $J$  splitting) when the inter-echo period is short relative to the inverse of the shift difference. The influence of this effect diminishes as  $1/(\pi\Delta\nu 2\tau)$ . In this study the majority of the  $^{29}\text{Si}$ – $^{29}\text{Si}$  pairs fall in the weak coupling limit and we show that only a small fraction (*vide infra*) are lost due to being in the strong coupling limit or having frequency shift differences that are small compared to  $1/(2\tau)$ .

## B. Pulse Sequence

The shifted-echo Phase Incremented Echo Train Acquisition (SE-PIETA) pulse sequence is shown in Fig. 1. We describe this sequence using the symmetry pathway formalism<sup>37</sup> which generalizes the concept of coherence transfer pathways<sup>38</sup> to the “spatial pathway,” which maps into a set of *spatial symmetry pathways*, and the “transition pathway,” which maps into a set of *transition symmetry pathways*. In the case of weak  $J$  coupling between



dilute  $^{29}\text{Si}$ - $^{29}\text{Si}$  pairs under fast magic-angle spinning (MAS) the rotating frame transition frequency is given by

$$\Omega_{AX} = -\omega_0\sigma_{\text{iso},A} \wp_A - \omega_0\sigma_{\text{iso},X} \wp_X - 2\pi J_{AX} \mathfrak{d}_{AX}, \quad (7)$$

where the transition symmetry functions are given by

$$\begin{aligned} \wp_A &= m_{A,j} - m_{A,i}, \\ \wp_X &= m_{X,j} - m_{X,i}, \\ \mathfrak{d}_{AX} &= m_{A,j}m_{X,j} - m_{A,i}m_{X,i}. \end{aligned} \quad (8)$$

Here  $\sigma_{\text{iso},A}$  and  $\sigma_{\text{iso},X}$  are the isotropic nuclear shieldings,  $\omega_0$  is the Larmor frequency and  $J_{AX}$  is the indirect coupling constant. The quantum numbers,  $m_A$  and  $m_X$ , are associated with a quantized energy levels of  $A$  and  $X$  nuclei, respectively, while  $i$  and  $j$  represents the initial and final energy state of the NMR transition. The  $\wp_A$ ,  $\wp_X$ , and  $\mathfrak{d}_{AX}$  values for single quantum transitions in a system of two weakly coupled spin 1/2 nuclei are shown in Fig. S1 of the Supplemental Material<sup>39</sup>. In the case of two weakly coupled homonuclear nuclei it is useful to define the additional transition symmetry function  $\wp_{AX} = \wp_A + \wp_X$ . The  $\wp_A$ ,  $\wp_X$ , and  $\mathfrak{d}_{AX}$  spin transition symmetry functions reflect their symmetry under the orthogonal rotation subgroup where simple rules hold under a  $\pi$  pulse, such as, the  $\mathfrak{d}_{AX}$  spin transition symmetry function is invariant, whereas,  $\wp_A$ ,  $\wp_X$  and  $\wp_{AX}$  spin transition symmetry functions change sign.

The SE-PIETA sequence separates and correlates the third frequency term in Eq. (7), the weak  $J$  coupling, with the isotropic  $^{29}\text{Si}$  chemical shifts of the first and second terms in Eq. (7). This sequence is based on the PIETA method for obtaining a 2D  $J$ -resolved spectrum in a “pseudo-single-scan” experiment<sup>31</sup>. “Single-scan” in the sense that the entire multi-dimensional time domain signal is acquired in a single acquisition, and “pseudo” because the separate “single-scan” signals must also be acquired along an rf pulse phase dimension. Sampling in the rf pulse phase dimension, however, need not increase the total experiment time since it is performed in lieu of conventional phase cycling and signal averaging.

The shifted-echo modification of the sequence eliminates a signal artifact when using the original PIETA experiment for 2D  $J$ -resolved spectroscopy which arises from an inability to acquire a full echo for the  $t_1 = 0$  ( $n = 1$ ) cross-section. Using the shifted-echo approach<sup>16,37</sup>,

in the case of 2D  $J$ -resolved spectroscopy, requires a simultaneous echo of both  $\mathbb{p}$  and  $\mathbb{d}$  transition symmetries at  $t_1 = 0$ . It is well known<sup>40–42</sup> that such a simultaneous echo in the case of two weakly coupling nuclei can be generated with the sequence

$$\text{equilibrate} - \frac{\pi}{2} - \tau - \pi - \tau - \frac{\pi}{2} - \tau - \pi - \tau \rightarrow \bullet \quad (9)$$

The first  $\pi/2$  pulse on a system of two weakly coupled spin 1/2 nuclei excites all eight single quantum transitions, shown in Fig. S1, which then evolves for a period  $\tau$ . Next, the  $\pi$  pulse converts the transition  $|m_{A,j}, m_{X,j}\rangle \langle m_{A,i}, m_{X,i}|$  entirely into the transition  $| -m_{A,j}, -m_{X,j}\rangle \langle -m_{A,i}, -m_{X,i}|$  leaving the number of transition pathways after the  $\pi$  pulse at eight. By the end of the second  $\tau$  period all chemical shift evolution phase on these 8 transition pathways refocus into an echo. At this point these eight transition pathways can be divided into two sets of four with the first set having the same negative  $J$  (or  $\mathbb{d}_{AX}$ ) evolution:

$$\begin{array}{cc} \underbrace{A_2^* \xrightarrow{\pi} A_1, \quad X_2^* \xrightarrow{\pi} X_1,}_{\mathbb{p}_{AX} = +1 \rightarrow -1} & \underbrace{A_1 \xrightarrow{\pi} A_2^*, \quad X_1 \xrightarrow{\pi} X_2^*}_{\mathbb{p}_{AX} = -1 \rightarrow +1} \\ 2\mathbb{d}_{AX} = -1 \rightarrow -1 & 2\mathbb{d}_{AX} = -1 \rightarrow -1 \end{array} \quad (10)$$

and the other set having the same positive  $J$  (or  $\mathbb{d}_{AX}$ ) evolution:

$$\begin{array}{cc} \underbrace{A_1^* \xrightarrow{\pi} A_2, \quad X_1^* \xrightarrow{\pi} X_2,}_{\mathbb{p}_{AX} = +1 \rightarrow -1} & \underbrace{A_2 \xrightarrow{\pi} A_1^*, \quad X_2 \xrightarrow{\pi} X_1^*}_{\mathbb{p}_{AX} = -1 \rightarrow +1} \\ 2\mathbb{d}_{AX} = +1 \rightarrow +1 & 2\mathbb{d}_{AX} = +1 \rightarrow +1 \end{array} \quad (11)$$

The second  $\pi/2$  pulse has the similar effect as in a solid echo experiment<sup>43</sup>, which is to transfer coherence only between single quantum transitions with opposite signs of  $\mathbb{d}_{AX}$ <sup>44</sup>. As the  $\mathbb{d}_{AX}$  values of transitions remain invariant under the second  $\pi$  pulse while the  $\mathbb{p}_{AX}$  symmetries refocus again into an echo there will be a simultaneous echo of both  $\mathbb{p}_{AX}$  and  $\mathbb{d}_{AX}$  symmetries at the end of the fourth  $\tau$  period as shown in Fig. 1. With perfect  $\pi/2$  and  $\pi$  rotations the transition pathways in two weakly coupled nuclei generate the simultaneous echo at  $t_1 = 0$  with no loss of intensity to other transition pathways.

After the formation of the simultaneous echo the chemical shift evolution can be continually refocused by a train of  $\pi$  pulses into echoes whose modulation by  $J$  evolution leads to the desired doublet splitting. The 16 detectable pathways with  $2\Delta\mathbb{d}_{AX} = +2$ , leading to the

$n^{\text{th}}$  echo is given in condensed notation below,

$$\left. \begin{array}{l} A_2^* \xrightarrow{\pi} A_1 \xrightarrow{\frac{\pi}{2}} \\ X_2^* \xrightarrow{\pi} X_1 \xrightarrow{\frac{\pi}{2}} \\ A_1 \xrightarrow{\pi} A_2^* \xrightarrow{\frac{\pi}{2}} \\ X_1 \xrightarrow{\pi} X_2^* \xrightarrow{\frac{\pi}{2}} \end{array} \right\} \otimes \left\{ \begin{array}{l} A_1^* [\xrightarrow{\pi} A_2(t_2) \xrightarrow{\pi} A_1^* ]_{\kappa}, \\ X_1^* [\xrightarrow{\pi} X_2(t_2) \xrightarrow{\pi} X_1^* ]_{\kappa}, \\ A_2 [\xrightarrow{\pi} A_1^* \xrightarrow{\pi} A_2(t_2) ]_{\kappa}, \\ X_2 [\xrightarrow{\pi} X_1^* \xrightarrow{\pi} X_2(t_2) ]_{\kappa}, \end{array} \right. \quad (12)$$

and the 16 detectable pathways with  $2\Delta d_{AX} = -2$ , leading to the  $n^{\text{th}}$  echo is similarly given by,

$$\left. \begin{array}{l} A_1^* \xrightarrow{\pi} A_2 \xrightarrow{\frac{\pi}{2}} \\ X_1^* \xrightarrow{\pi} X_2 \xrightarrow{\frac{\pi}{2}} \\ A_2 \xrightarrow{\pi} A_1^* \xrightarrow{\frac{\pi}{2}} \\ X_2 \xrightarrow{\pi} X_1^* \xrightarrow{\frac{\pi}{2}} \end{array} \right\} \otimes \left\{ \begin{array}{l} A_2^* [\xrightarrow{\pi} A_1(t_2) \xrightarrow{\pi} A_2^* ]_{\kappa}, \\ X_2^* [\xrightarrow{\pi} X_1(t_2) \xrightarrow{\pi} X_2^* ]_{\kappa}, \\ A_1 [\xrightarrow{\pi} A_2^* \xrightarrow{\pi} A_1(t_2) ]_{\kappa}, \\ X_1 [\xrightarrow{\pi} X_2^* \xrightarrow{\pi} X_1(t_2) ]_{\kappa}, \end{array} \right. \quad (13)$$

where  $t_2$  next to a transition represent acquisition of an echo. A full expansion of these 32 transition pathways are given in the Supplemental Material<sup>39</sup>.

The symmetry pathways associated with these transition pathways are

$$\begin{aligned} \mathbb{P}_{AX} &= 0 \xrightarrow{\frac{\pi}{2}} +1 \xrightarrow{\pi} -1 \xrightarrow{\frac{\pi}{2}} +1 [\xrightarrow{\pi} -1(t_2) \xrightarrow{\pi} +1 ]_{\kappa}, \\ 2d_{AX} &= 0 \xrightarrow{\frac{\pi}{2}} \mp 1 \xrightarrow{\pi} \mp 1 \xrightarrow{\frac{\pi}{2}} \pm 1 [\xrightarrow{\pi} \pm 1(t_2) \xrightarrow{\pi} \pm 1 ]_{\kappa}, \end{aligned} \quad (14)$$

$$\begin{aligned} \mathbb{P}_{AX} &= 0 \xrightarrow{\frac{\pi}{2}} +1 \xrightarrow{\pi} -1 \xrightarrow{\frac{\pi}{2}} -1 [\xrightarrow{\pi} +1 \xrightarrow{\pi} -1(t_2) ]_{\kappa}, \\ 2d_{AX} &= 0 \xrightarrow{\frac{\pi}{2}} \mp 1 \xrightarrow{\pi} \mp 1 \xrightarrow{\frac{\pi}{2}} \pm 1 [\xrightarrow{\pi} \pm 1 \xrightarrow{\pi} \pm 1(t_2) ]_{\kappa}, \end{aligned} \quad (15)$$

$$\begin{aligned} \mathbb{P}_{AX} &= 0 \xrightarrow{\frac{\pi}{2}} -1 \xrightarrow{\pi} +1 \xrightarrow{\frac{\pi}{2}} +1 [\xrightarrow{\pi} -1(t_2) \xrightarrow{\pi} +1 ]_{\kappa}, \\ 2d_{AX} &= 0 \xrightarrow{\frac{\pi}{2}} \mp 1 \xrightarrow{\pi} \mp 1 \xrightarrow{\frac{\pi}{2}} \pm 1 [\xrightarrow{\pi} \pm 1(t_2) \xrightarrow{\pi} \pm 1 ]_{\kappa}, \end{aligned} \quad (16)$$

$$\begin{aligned} \mathbb{P}_{AX} &= 0 \xrightarrow{\frac{\pi}{2}} -1 \xrightarrow{\pi} +1 \xrightarrow{\frac{\pi}{2}} -1 [\xrightarrow{\pi} +1 \xrightarrow{\pi} -1(t_2) ]_{\kappa}, \\ 2d_{AX} &= 0 \xrightarrow{\frac{\pi}{2}} \mp 1 \xrightarrow{\pi} \mp 1 \xrightarrow{\frac{\pi}{2}} \pm 1 [\xrightarrow{\pi} \pm 1 \xrightarrow{\pi} \pm 1(t_2) ]_{\kappa}. \end{aligned} \quad (17)$$

Because the second  $\pi/2$  must allow both  $\Delta p_{AX} = 0$  and  $\Delta p_{AX} = \pm 2$  it is necessary to implement separate phase dimensions for the preparation sequence of Eq. (9) and the echo train acquisition as shown in Fig. 1. A Fourier transform of the signal,  $s(\phi_1, \phi_2, n, t_2)$ , with respect to the pulse phases  $\phi_1$  and  $\phi_2$  transforms the signal to  $s'(\Delta p_1, \Delta p_2, n, t_2)$  signal where the two desired pathway signals at  $n^{\text{th}}$  echo appear at the coordinates

$$\begin{aligned} \{\Delta p_1, \Delta p_2\}_n &= \{3 (-1)^{n-1}, 2 (-1)^n \lceil n/2 \rceil\}, \\ \{\Delta p_1, \Delta p_2\}_n &= \{5 (-1)^n, 2 (-1)^n \lceil n/2 \rceil\}. \end{aligned} \quad (18)$$

Here  $\Delta p_1$  is the accumulated change in coherence order through the first three pulses while  $\Delta p_2$  is the accumulated change in coherence order through the subsequent  $\pi$  pulses leading up to the  $n^{\text{th}}$  echo and  $\lceil \cdot \rceil$  is the ceiling function. Because desired signal along  $\Delta p_1$  dimension is always sampled at either  $\pm 3$  or  $\pm 5$  for all  $n$ , we show in the Supplemental Material<sup>39</sup> an improved pulse sequence where the  $\phi_1$  phase dimension is replaced by a phase cycling scheme.

### III. METHODS AND ANALYSIS

#### A. Sample Preparation

The glass was synthesized starting from  $\text{SiO}_2$  (99.7 % Strem Chemicals) and Cobalt (II) carbonate hydrate ( $\text{CoCO}_3 \cdot x\text{H}_2\text{O}$ ) (99.99% Aldrich). The latter was first heat-treated in an alumina crucible for one hour at  $800^\circ\text{C}$  to eliminate anionic impurities (and  $\text{H}_2\text{O}$ ). The same heat treatment was applied after the mixing and before melting. The mixed starting components were melted for approximately 2 min on a water-cooled aluminum plate connected to a vertical laboratory solar furnace of 2 kW power and heat flux of 900-1000  $\text{W}/\text{m}^2$ . Within a few seconds the temperature reached around  $1900^\circ\text{C}$  ( $\pm 50^\circ\text{C}$ ) and instantaneous melting was observed without the formation of bubbles or any visible precipitates. Some fumes were observed, indicating vaporization of  $\text{SiO}_2$ , which are expected in an oxidizing atmosphere<sup>45</sup>. Transparent quasi-spherical blue glassy droplets between 2-5 mm in diameter were obtained after melting. The glass composition was determined by SEM-EDX analysis (Hitachi S 4500, EDS: Kevex) after a metallization with gold using the beam energy of 20 keV. With no cobalt signal detected, its amount is estimated to be less than a few 100 ppm.

## B. NMR Spectroscopy

The experiment was performed on a Bruker Avance III HD 400 MHz NMR spectrometer operating at 9.4 T, with a  $^{29}\text{Si}$  Larmor frequency of 79.40716 MHz, using a 4 mm rotor spinning at 14.286 kHz. The chemical shift was referenced with respect to TMS at 0 ppm. The radio-frequency field strength was set to 53.7 kHz with a  $t_{90^\circ}$  of 4.65  $\mu\text{s}$ . The magic angle was set accurately to within  $0.002^\circ$  using STMAS<sup>46,47</sup> on  $\text{RbNO}_3$ . This procedure provides better accuracy than the KBr spinning sidebands based procedure and removes residual  $^{29}\text{Si}$ - $^{29}\text{Si}$  dipolar couplings in the  $^{29}\text{Si}$  2D  $J$ -resolved experiments.

The four dimensional pulse sequence shown in Fig. 1 was implemented, with a time dimension,  $t_2$ , an echo count dimension,  $n$ , and two phase dimensions  $\phi_1$  and  $\phi_2$ . The pulse phase increment was set to  $\pi/6$  and  $\pi/128$  for the phase dimensions,  $\phi_1$  and  $\phi_2$ , with 12 and 256 phase points, respectively. A total of 254 echoes were collected with a recovery period of 60 s. The dwell time was set at 40  $\mu\text{s}$ . The inter-echo period,  $2\tau$ , was set to 40 ms. A total of 16 scans were averaged for a total experiment time of 40 days. The Bruker pulse sequence for the shifted-echo PIETA sequence is available in the Supplemental Material<sup>39</sup>.

## C. Signal processing

All signal processing was performed with *RMN*<sup>48</sup>. A two dimensional Fourier transform was performed on the four dimensional signal,  $s(\phi_1, \phi_2, n, t_2)$ , with respect to the two phase dimensions,  $\phi_1$  and  $\phi_2$ , transforming to  $s'(\Delta p_1, \Delta p_2, n, t_2)$ . The signal corresponding to the desired  $\{\Delta p_1, \Delta p_2\}_n$  coordinates in Eq. (18) were retained in  $s'(\Delta p_1, \Delta p_2, n, t_2)$  whereas signal at all other  $\{\Delta p_1, \Delta p_2\}_n$  coordinates were zeroed. Next, a projection onto the  $\Delta p_1$  dimension followed by a projection onto  $\Delta p_2$  dimension was performed. From the resulting two dimensional echo count  $n$  vs time  $t_2$  signal,  $s''(n, t_2)$ , the echo count dimension  $n$  was converted to the echo time dimension,  $t_1$ , using the relationship

$$t_1 = 2\tau(n - 1). \quad (19)$$

The formation of simultaneous  $\text{p}_{AX}$  and  $\text{d}_{AX}$  echo occurs at  $t_1 = t_2 = 0$ . A step-by-step graphical illustration of this processing is given in the Supplemental Material<sup>39</sup>. Alternatively, a Matlab script that performs a post-acquisition “phase cycling” down to a conventional 2D  $J$ -resolved signal,  $s''(t_1, t_2)$  is also made available in the Supplemental Material<sup>39</sup>.

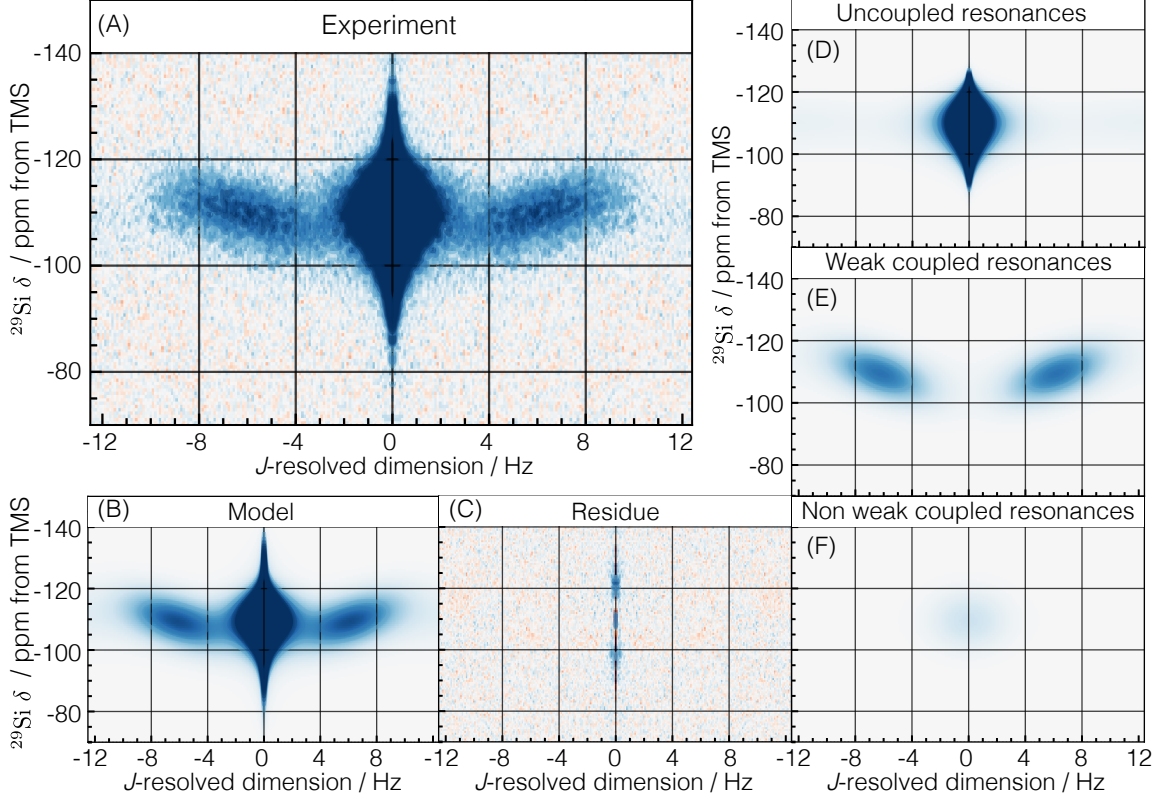


FIG. 2. (A) Natural abundance  $^{29}\text{Si}$ -O- $^{29}\text{Si}$  2D  $J$ -resolved spectrum of CoO doped silica glass showing contributions from both coupled and uncoupled  $^{29}\text{Si}$  resonances. (B) Simulation and (C) residue obtained from the least square minimization of experimental data using model  $s(\delta, t_1)$  in Eq (25). (D-F) Decomposition of the Fourier transform of the model  $s(\delta, t_1)$  in Eq. (25) into (D) uncoupled  $^{29}\text{Si}$  spin resonances, (E) weakly coupled  $^{29}\text{Si}$ -O- $^{29}\text{Si}$  spin resonances and (F) non weakly coupled  $^{29}\text{Si}$ -O- $^{29}\text{Si}$  spin resonances.

A two dimensional Fourier transform was performed on  $s''(t_1, t_2)$ , transforming the time dimension,  $t_2$  into the  $^{29}\text{Si}$  MAS dimension and echo time dimension,  $t_1$ , into the  $J$ -resolved dimension. Next, a shear of  $-45^\circ$  was performed along the  $^{29}\text{Si}$  MAS dimension to transform it into a pure  $^{29}\text{Si}$  isotropic chemical shift dimension,  $\delta$ . The resulting  $^{29}\text{Si}$  2D  $J$ -resolved spectrum is shown in Fig. 2A.

#### D. $^{29}\text{Si}$ Isotopomer Statistics

Of the three stable isotopes of silicon,  $^{28}\text{Si}$  is the most abundant at 92.23%, followed by  $^{29}\text{Si}$  at 4.67%, and  $^{30}\text{Si}$  at 3.1%. Of these only  $^{29}\text{Si}$  is NMR active with  $I = 1/2$ . To predict the relative intensity of all possible  $J$  multiplets in the  $^{29}\text{Si}$  NMR spectrum of silica glass we start with the probability that  $n$  of the four Si atoms connected to a  $^{29}\text{SiO}_4$  tetrahedron in silica glass are  $^{29}\text{Si}$  nuclei,

$$P_n = \binom{4}{n} p^n (1-p)^{(4-n)}, \quad (20)$$

where  $p = 0.0467$  is the natural abundance of  $^{29}\text{Si}$ . This expression predicts that the relative intensity of  $J$  multiplets decrease rapidly with increasing  $n$ , with  $P_0 = 0.826$  for the uncoupled resonance,  $P_1 = 0.162$  for the two spin multiplet,  $P_2 = 0.0119$  for the three spin multiplet,  $P_3 = 0.000388$  for the four spin multiplet, and  $P_4 = 4.76 \times 10^{-6}$  for the five spin multiplet. While the  $^{29}\text{Si}$  NMR spectrum of silica glass contains contributions from all five cases we can confidently take the observed intensity as arising entirely from the uncoupled and two spin doublet resonances. Thus while the sum of the  $P_n$  is 1 we can approximately terminate the sum at  $P_1$ :

$$\sum_n P_n \approx P_0 + P_1 \approx 1. \quad (21)$$

In Eq. (7) and section II, we considered the resonances from an ideal case of two weakly  $J$ -coupled spin 1/2 nuclei where the only interactions were isotropic chemical shifts of the two nuclei and the  $J$  coupling between them. In the solid state, however, the chemical shift anisotropies (CSA) and dipolar couplings also play an important role in the detection of  $J$ -couplings. In a simple Hahn echo experiment a two coupled spin system in the solid state behaves identical to that of solution state NMR<sup>49</sup> in the fast MAS limit<sup>50</sup> where

$$|\nu_r| > |d\Delta\nu/2\pi J|, |\Delta\nu_{\text{iso}}|. \quad (22)$$

Here  $\nu_r$  is the spinning frequency,  $d/2\pi$  is the instantaneous dipole-dipole coupling frequency,  $\Delta\nu$  is the difference in the instantaneous chemical shift frequencies,  $J$  is the scalar coupling frequency and  $\Delta\nu_{\text{iso}}$  is the difference in the isotropic chemical shift frequencies of the connected nuclei. On the other hand, under moderate MAS speeds<sup>50</sup>,

$$|\Delta\nu_{\text{iso}}| \lesssim |\Delta\nu_{\text{ansio}}| < |\nu_r| < |d\Delta\nu/2\pi J| \quad (23)$$

the coupled spins mostly remain within a weak coupling limit because the CSA ensures that the instantaneous chemical shifts of the coupled spins are different for most of the time even when the two spins have identical isotropic chemical shifts. In Eq. (23),  $\Delta\nu_{\text{ansio}}$  is the differences in the anisotropic part of the instantaneous chemical shift frequencies.

Because of the disordered network in silica glass, there is a distribution of isotropic chemical shifts as well as CSAs, dipole-dipole and  $J$  couplings. In silica glass, the  $Q^4$  chemical shift anisotropy<sup>51</sup> is of the order of 2 kHz, the dipole-dipole coupling frequency between two  $^{29}\text{Si}$  at 3 Å is of the order of 170 Hz, the isotropic chemical shift spans a range of over 2 kHz, and the  $J$ -coupling varies from 5 to 25 Hz. With  $\nu_r = 14.286$  kHz, most of the coupled spin system in silica glass would reside within the moderate MAS condition, Eq. (23), and would result in echoes that are modulated by  $J$ -coupling as  $\cos \pi Jt$ , i.e., the weak coupling limit. Given the strength of all interactions in silica glass, some fraction of the coupled spins—more likely for the higher  $J$ -couplings—may be in fast MAS limit, in which case, there will be a finite probability of non-weak couplings. To account for these non-weak resonances we split the doublet relative intensity into

$$P_1 \approx P_{a_0} + P_{a_1}, \quad (24)$$

where  $P_{a_0}$  is the relative intensity of weakly coupled  $^{29}\text{Si}$ -O- $^{29}\text{Si}$  spins, and  $P_{a_1}$  is the relative intensity of non-weak couplings.

### E. Line shape analysis

As a starting point in our 2D line shape analysis we define  $p(J, \delta)$  as the bi-variate probability distribution for isotropic  $^{29}\text{Si}$  chemical shift and  $^2J_{\text{Si-O-Si}}$  coupling in silica glass. The observed signal can be decomposed into a weighted sum of three contributions from (1) uncoupled  $^{29}\text{Si}$  sites, (2) weakly coupled  $^{29}\text{Si}$ -O- $^{29}\text{Si}$  sites and (3) non-weakly coupled  $^{29}\text{Si}$ -O- $^{29}\text{Si}$  sites,

$$s(\delta, t_1) = (1 - P_{a_0} - P_{a_1})s_1(\delta, t_1) + P_{a_0}s_2(\delta, t_1) + P_{a_1}s_3(\delta, t_1), \quad (25)$$

where the weights are constrained by the natural abundance  $^{29}\text{Si}$  statistics of Eq. (21) and (24).



The first contribution,  $s_1(\delta, t)$ , from uncoupled  $^{29}\text{Si}$  resonances, is modeled as the product

$$s_1(\delta, t_1) = p(\delta)s_{\text{decay}}(\delta, t_1), \quad (26)$$

where  $p(\delta)$  is the one-dimensional probability distribution for isotropic  $^{29}\text{Si}$  chemical shift of silica glass, given by

$$p(\delta) = \int_J p(J, \delta)dJ, \quad (27)$$

and  $s_{\text{decay}}(\delta, t_1)$  is a stretched exponential decay in the echo time dimension,  $t_1$ , associated with each isotropic chemical shift. The isotropic  $^{29}\text{Si}$  line shape of silica glass has been well established<sup>9,51–53</sup> as a skewed distribution. Of the various models that have been proposed to describe this line shape<sup>52</sup>, the skew-normal distribution<sup>51,54</sup> has been found to be reasonably accurate. In our analysis, however, any small inaccuracy is of concern because, as stated earlier, the coupled  $^{29}\text{Si}$ -O- $^{29}\text{Si}$  resonances only accounts for 16.2% of the total observable resonances. Therefore, any residual modulation from inaccuracies in modeling the uncoupled isotropic  $^{29}\text{Si}$  line shape will cause a significant distortion in the extracted  $^2J$  doublet line shape. Thus, we introduce additional flexibility into the isotropic  $^{29}\text{Si}$  uncoupled line shape model with a combination of skew-normal and normal distribution function

$$p(\delta) \approx \underbrace{\frac{C_1}{\Delta_1} e^{-Y_1^2} \{1 + \text{erf}(\alpha_1 Y_1)\}}_{\text{skew-normal}} + \underbrace{\frac{C_2}{\Delta_2} e^{-Y_2^2}}_{\text{normal}}, \quad (28)$$

where

$$Y_i = \frac{\delta - \xi_i}{\sqrt{2}\Delta_i}, \quad (29)$$

and  $C_i$ ,  $\xi_i$ ,  $\Delta_i$  and  $\alpha_i$  are the amplitude, location, scale and shape parameters, respectively, for the  $i^{\text{th}}$  distribution. This model gives good agreement with the observed isotropic  $^{29}\text{Si}$  line shape, as shown in Fig. S9 of the Supplemental Material<sup>39</sup>. The familiar moments of this distribution: mean isotropic chemical shift,  $\mu_{\text{mas}}$ , the standard deviation,  $\sigma_{\text{mas}}$ , the skewness,  $\gamma_{\text{mas}}$ , and the excess kurtosis,  $\kappa_{\text{mas}}$ , are listed in Table I.

It is well established that NMR relaxation behavior in glasses, specifically low abundance nuclei like  $^{29}\text{Si}$ , are often found to be stretched exponentials with a stretch exponent of  $\beta \approx 0.5$ —the hallmark of a continuous distribution of relaxation times arising from distant and fluctuating paramagnetic centers<sup>55</sup>. Considering paramagnetic relaxation to be the only dominant mechanism in the silica glass used in our measurement, doped with CoO where Co

moments	description	value
$\mu_{\text{mas}} = \mu_1$	mean	-109.63 ppm
$\sigma_{\text{mas}} = \sqrt{\mu_2}$	standard deviation	6.45 ppm
$\gamma_{\text{mas}} = \mu_3/\sigma_{\text{mas}}^3$	skewness	0.06
$\kappa_{\text{mas}} = \mu_4/\sigma_{\text{mas}}^4 - 3$	excess kurtosis	1.42

TABLE I. Moment analysis of uncoupled  $^{29}\text{Si}$  isotropic MAS line shape from model  $p(\delta)$  in Eq. (28) where  $\mu_n$  is the  $n^{\text{th}}$  moment.

is the paramagnetic center, we expect a similar stretch exponential behavior for the signal decay along the echo time dimension. We further observe a differential stretch exponential relaxation across  $^{29}\text{Si}$  isotropic chemical shift sites ranging from -95 ppm to -125 ppm with a slight linear variation in the stretch exponent from 0.6 to 0.5, respectively. This is modeled as

$$s_{\text{decay}}(\delta, t_1) = \exp \left\{ - \left( \frac{t_1 + 4\tau}{T_2} \right)^{\beta(\delta)} \right\}, \quad (30)$$

where the stretch exponent is given by

$$\beta(\delta) = c_\beta + m_\beta (\delta - \mu_\delta), \quad (31)$$

with  $c_\beta$  and  $m_\beta$  as the corresponding intercept and slope, respectively, and  $T_2$  is the transverse dephasing time constant. The term  $4\tau$  is added in Eq. (30) because  $t_1$  is referenced to zero at the first echo whereas the signal starts relaxing after the first  $\pi/2$  pulse, i.e., a period of  $4\tau$  before the detection of first echo. Here,  $\mu_\delta$  is the mean  $^{29}\text{Si}$  isotropic chemical shift.

The second echo train signal contribution,  $s_2(\delta, t_1)$ , from the weakly coupled  $^{29}\text{Si}$ -O- $^{29}\text{Si}$  resonances for a given chemical shift is given by

$$s_2(\delta, t_1) = \left[ \int_J p_w(J, \delta) \cos(\pi J t_1) dJ \right] s_{\text{decay}}(\delta, t_1), \quad (32)$$

where  $p_w(J, \delta)$  is the bi-variate probability distribution of  $^2J_{\text{Si-O-Si}}$  couplings and isotropic chemical shifts from the weakly coupled  $^{29}\text{Si}$  nuclei in silica glass. For  $s_2(\delta, t_1)$  we find it sufficient to approximate  $p_w(J, \delta)$  as a bi-variate normal distribution with a correlation coefficient  $r_{J,\delta}$ . One can then express  $s_2(\delta, t_1)$  (see Supplemental Material<sup>39</sup>) as

$p(\delta)$		$s_{\text{decay}}(\delta, t)$		$p(J, \delta)$		$s_3(\delta, t)$	
$C_1$	$(4.21 \pm 0.01) \times 10^7$	$C_2$	$(4.5 \pm 0.1) \times 10^6$	$T_2$	$P_{a_0}$	$P_{a_1}$	0.018
$\xi_1$	$-114.16 \pm 0.01$ ppm	$\xi_2$	$-109.7 \pm 0.2$ ppm	$c_\beta$	$\sigma_J$	$\mu_\delta$	$-109.57 \pm 0.05$ ppm
$\Delta_1$	$7.25 \pm 0.01$ ppm	$\Delta_2$	$11.8 \pm 0.2$ ppm	$m_\beta$	$\mu_J$	$\sigma_\delta$	$6.2 \pm 0.04$ ppm
$\alpha_1$	$1.283 \pm 0.008$		$(0.00326 \pm 0.00005)/\text{ppm}$		$r_{J,\delta}$	$\sigma_s$	$3.3 \pm 0.2$ Hz
$\chi_r^2 = 2.5$							

TABLE II. Optimized fit parameters and reduced chi square,  $\chi_r^2$ , from least square minimization of the residuals using model in Eq. (25). The reported uncertainties are twice the standard deviation.

$$s_2(\delta, t_1) = \underbrace{\frac{N}{\sigma_\delta} \exp \left[ -\frac{(\delta - \mu_\delta)^2}{2\sigma_\delta^2} \right]}_{\text{coupled } ^{29}\text{Si lineshape}} \underbrace{\exp \left[ -\frac{1}{2}\pi^2 t_1^2 \sigma_J^2 (1 - r_{J,\delta}^2) \right]}_{J\text{-distribution}} \cos(\pi t_1 J(\delta)) s_{\text{decay}}(\delta, t_1), \quad (33)$$

where  $N = [C_1 + C_2]$  and

$$J(\delta) = r_{J,\delta} \frac{\sigma_J}{\sigma_\delta} (\delta - \mu_\delta) + \mu_J. \quad (34)$$

The first part in Eq. (33) refers to the  $^{29}\text{Si}$  isotropic chemical shift lineshape arising from coupled  $^{29}\text{Si}$ -O- $^{29}\text{Si}$  resonances and is described by a normal distribution with mean  $\mu_\delta$  and standard deviation  $\sigma_\delta$ . The second part describes a normal distribution of  $J$ -coupling with mean  $\mu_J$  and standard deviation  $\sigma_J$ . The cosine term describes the time domain oscillation and  $s_{\text{decay}}(\delta, t)$  simulates the signal decay as given in Eq. (30).

Similarly, the third contribution,  $s_3(\delta, t_1)$ , from the non-weakly coupled  $^{29}\text{Si}$ -O- $^{29}\text{Si}$  resonances, is modeled as the product

$$s_3(\delta, t_1) = \underbrace{\frac{N}{\sigma_\delta} \exp \left[ -\frac{(\delta - \mu_\delta)^2}{2\sigma_\delta^2} \right]}_{\text{coupled } ^{29}\text{Si lineshape}} \exp \left[ -\frac{\pi^2 \sigma_s^2 t_1^2}{2} \right] s_{\text{decay}}(\delta, t_1) \quad (35)$$

which shares the same  $^{29}\text{Si}$  isotropic chemical shift lineshape as the weakly coupled resonances, and experiences an additional decay during the echo time which follows a Gaussian dependence with standard deviation  $\sigma_s$ .

The experimental data was subjected to a least squares minimization with the full model of Eq. (25) using python's LMFIT<sup>56</sup> module. All data modeling and spectral analysis were performed with code written in python 3<sup>57</sup>. The graphics were produced using python's matplotlib library<sup>58</sup>. The optimized fit parameters along with reduced chi square are listed in Table II. Note that the mean and standard deviation in Tables I and II, for the uncoupled and coupled isotropic line shapes, respectively, are approximately identical. The best-fit simulation and residuals after a Fourier transformation along the echo time dimension,  $t_1$ , are presented in Fig. 2.

## F. Mapping to Si-O-Si bond angle distribution

The dependence of the  $^2J_{\text{Si-O-Si}}$  coupling on local structure in two connected Q<sup>4</sup> was recently examined using first-principles DFT calculations<sup>32</sup>. The two main influences on

coefficient	value	coefficient	value
$a_J$	107.88°	$b_J$	223.49°
$c_J$	0.00002487°	$d_J$	53.01
$m_1$	0.778 Hz/°	$J_0$	-7.5 Hz
$a_\delta$	-0.6148 ppm/°	$b_\delta$	-19.297 ppm

TABLE III. Coefficients used in Eqs. (40) and (38) for mapping the mean chemical shift and  ${}^2J_{\text{Si-O-Si}}$  coupling into the double mean Si-O-Si angle of the two  $Q^4$  involved in coupling and the linkage Si-O-Si angle of the two coupled nuclei.

${}^2J_{\text{Si-O-Si}}$  were found to be a primary dependence on the linkage Si-O-Si angle and a secondary dependence on a double mean of Si-O-Si linkage angles of the two connecting tetrahedra  $Q_i^4$  and  $Q_j^4$  containing the coupled  ${}^{29}\text{Si}$  nuclei. Here, the double mean is given by

$$\overline{\langle \Omega \rangle} = \frac{\langle \Omega \rangle_i + \langle \Omega \rangle_j}{2} = \frac{1}{8} \left( 2\Omega_0 + \sum_{k=1}^6 \Omega_k \right), \quad (36)$$

where  $\langle \Omega \rangle_i$  and  $\langle \Omega \rangle_j$  are mean Si-O-Si bond angles at  $Q_i^4$  and  $Q_j^4$ , respectively, and given by

$$\langle \Omega \rangle_i = \frac{1}{4} \sum_{k=0,1,2,3} \Omega_k, \quad \text{and} \quad \langle \Omega \rangle_j = \frac{1}{4} \sum_{k=0,4,5,6} \Omega_k. \quad (37)$$

In this numbering scheme the six outer Si-O-Si linkage angles correspond to  $k \neq 0$ . Following these definitions the  ${}^2J_{\text{Si-O-Si}}$  can be related to the  $Q_i^4$ - $Q_j^4$  inter-tetrahedral linkage angle,  $\Omega_0$ , according to

$$\Omega_0(J, \overline{\langle \Omega \rangle}) = a_J + b_J \left( \frac{J - J_0}{m_1 \overline{\langle \Omega \rangle}} \right) + c_J \exp \left\{ d_J \left( \frac{J - J_0}{m_1 \overline{\langle \Omega \rangle}} \right) \right\}. \quad (38)$$

The coefficients  $a_J$ ,  $b_J$ ,  $c_J$ ,  $d_J$ ,  $J_0$  and  $m_1$  determined previously<sup>32</sup>, are given in Table III. Note that this expression requires both  ${}^2J_{\text{Si-O-Si}}$  and the double mean,  $\overline{\langle \Omega \rangle}$  of the  $Q_i^4$ - $Q_j^4$  pair to determine  $\Omega_0$ .

There is an established linear relationship<sup>53,59,60</sup> between  ${}^{29}\text{Si}$  isotropic chemical shift  $\delta$  of a  $Q^4$  site and its mean Si-O-Si angle,

$$\langle \Omega \rangle = (\delta - b_\delta)/a_\delta, \quad (39)$$

with coefficients,  $a_\delta$  and  $b_\delta$ , given in Table III. From this one readily obtains

$$\overline{\langle \Omega \rangle} = (\bar{\delta} - b_\delta)/a_\delta, \quad (40)$$

where  $\bar{\delta} = \frac{1}{2}(\delta_i + \delta_j)$  is the mean  $^{29}\text{Si}$  isotropic chemical shift, and  $\delta_i$  and  $\delta_j$  are the  $^{29}\text{Si}$  isotropic chemical shifts of  $\text{Q}_i^4$  and  $\text{Q}_j^4$ , respectively. Thus, Eqs. (38) and (40) can be combined to map  $p(J, \bar{\delta})$  into  $p(\Omega_0, \overline{\langle \Omega \rangle})$ . While this mapping requires  $p(J, \bar{\delta})$ , the line shape analysis of the 2D  $J$ -resolved spectrum only provides  $p_w(J, \delta)$ . To proceed it is necessary to make the approximation  $p(J, \delta) \approx p_w(J, \delta)$ . Based on the values of  $P_{a_0} = 0.144$  and  $P_{a_1} = 0.018$  from the experimental line shape analysis this would suggest a loss of intensity due to the non-weakly coupled sites as 11.1%. This loss will be strongest at the highest  $J$ -couplings. Therefore, this approximation is likely to reduce intensity in the Si-O-Si bond angle distribution at the higher angles. Note, that this loss can be diminished by performing measurements at higher magnetic field strengths and using longer inter-echo periods.

We begin the analysis by determining  $p(J, \bar{\delta})$  from  $p(J, \delta)$  through the coordinate transformations

$$\text{Series A: } p(J, \delta) \xrightarrow{A1} p(J, \delta_i, \delta_j) \xrightarrow{A2} p(J, \bar{\delta}).$$

*Step A1:* Given that  $p(J, \delta)$  is approximately a bi-variate normal distribution we assume that we can construct  $p(J, \delta_i, \delta_j)$ , a trivariate normal distribution of silica glass, imposing the restrictions that

$$\begin{aligned} p(\delta_i) &= \int p(J, \delta_i, \delta_j) dJ d\delta_j = \int p(J, \delta) dJ = p(\delta), \\ p(\delta_j) &= \int p(J, \delta_i, \delta_j) dJ d\delta_i = \int p(J, \delta) dJ = p(\delta). \end{aligned}$$

This leads to a covariance matrix for  $p(J, \delta_i, \delta_j)$  given by

$$\mathbf{V}_{J, \delta_i, \delta_j} = \begin{bmatrix} \sigma_J^2 & r_{J, \delta} \sigma_J \sigma_\delta & r_{J, \delta} \sigma_J \sigma_\delta \\ r_{J, \delta} \sigma_J \sigma_\delta & \sigma_\delta^2 & r_{\delta_i, \delta_j} \sigma_\delta^2 \\ r_{J, \delta} \sigma_J \sigma_\delta & r_{\delta_i, \delta_j} \sigma_\delta^2 & \sigma_\delta^2 \end{bmatrix}, \quad (41)$$

and a mean vector of  $\boldsymbol{\mu}_{J, \delta_i, \delta_j} = [\mu_J, \mu_\delta, \mu_\delta]^T$  where the superscript  $T$  represents the transpose. The only unknown parameter in the covariance matrix  $\mathbf{V}_{J, \delta_i, \delta_j}$  is the correlation coefficient,  $-1 \leq r_{\delta_i, \delta_j} \leq 1$ , between the  $^{29}\text{Si}$  isotropic chemical shift distributions  $p(\delta_i)$  and  $p(\delta_j)$ .

Since  $\text{Q}_i^4$  and  $\text{Q}_j^4$  share a common angle, i.e.,  $\Omega_0$ , their mean angle distributions,  $p(\langle \Omega \rangle_i)$  and  $p(\langle \Omega \rangle_j)$ , will be correlated even when the individual bond angle distributions, i.e.,  $p(\Omega_k)$ ,

are uncorrelated. In the appendix we derive approximate expected relationships between the variances and covariances of  $\Omega_0$ ,  $\langle\Omega\rangle_i$ ,  $\langle\Omega\rangle_j$ , and  $\overline{\langle\Omega\rangle}$  with an initial assumption of a seven dimensional normal distribution correlating all seven angles. In this assumption we further take the individual bond angle distributions,  $p(\Omega_k)$ , as identical, and correlated to each other with correlation coefficient  $r$  if the Si-O-Si bond angles share a Si, and with correlation coefficient  $r'$  if not. This leads to a covariance matrix for the bivariate distribution,  $p(\langle\Omega\rangle_i, \langle\Omega\rangle_j)$ , given by

$$\mathbf{V}_{\langle\Omega\rangle_i, \langle\Omega\rangle_j} = \frac{\sigma_\Omega^2}{4} \begin{bmatrix} (3r+1) & \frac{1}{4}(6r+9r'+1) \\ \frac{1}{4}(6r+9r'+1) & (3r+1) \end{bmatrix}, \quad (42)$$

where  $\sigma_\Omega^2$  is the variance of the individual bond-angle distribution. The corresponding correlation coefficient is given by

$$r_{\langle\Omega\rangle_i, \langle\Omega\rangle_j} = \frac{6r+9r'+1}{4(3r+1)}. \quad (43)$$

From this expression one can show that uncorrelated individual bond angle distributions, i.e.,  $r=r'=0$ , leads to a correlation coefficient between the two mean angle distributions of  $r_{\langle\Omega\rangle_i, \langle\Omega\rangle_j} = 0.25$ . The linear relationship between  $\delta$  and  $\langle\Omega\rangle$  leads to

$$r_{\delta_i, \delta_j} = r_{\langle\Omega\rangle_i, \langle\Omega\rangle_j}. \quad (44)$$

Thus, we expect  $r_{\delta_i, \delta_j} = 0.25$  when the individual bond angle distributions, i.e.,  $p(\Omega_k)$  are uncorrelated.

Similarly, the seven dimensional normal distribution also leads to the covariance matrix for the bivariate distribution,  $p(\Omega_0, \overline{\langle\Omega\rangle})$ , given by

$$\mathbf{V}_{\Omega_0, \overline{\langle\Omega\rangle}} = \sigma_\Omega^2 \begin{bmatrix} 1 & \frac{1}{4}(3r+1) \\ \frac{1}{4}(3r+1) & \frac{1}{32}(18r+9r'+5) \end{bmatrix}, \quad (45)$$

with a corresponding correlation coefficient given by

$$r_{\Omega_0, \overline{\langle\Omega\rangle}} = \frac{\sqrt{2}(3r+1)}{\sqrt{18r+9r'+5}}. \quad (46)$$

We will refer back to these last two results in later steps of this analysis.

*Step A2:* The distribution  $p(J, \delta_i, \delta_j)$  is mapped to distribution  $p(J, \bar{\delta})$  following the linear coordinate transformation

$$\begin{bmatrix} J \\ \bar{\delta} \end{bmatrix} = \underbrace{\begin{bmatrix} 1 & 0 & 0 \\ 0 & \frac{1}{2} & \frac{1}{2} \end{bmatrix}}_{\mathbf{A}_1} \begin{bmatrix} J \\ \delta_i \\ \delta_j \end{bmatrix}, \quad (47)$$

where  $\mathbf{A}_1$  is the projection matrix that projects the distribution  $p(J, \delta_i, \delta_j)$  onto the diagonal  $\delta_i = \delta_j$ . The mean vector of the  $p(J, \bar{\delta})$  distribution becomes

$$\boldsymbol{\mu}_{J, \bar{\delta}} = \mathbf{A}_1 \cdot \boldsymbol{\mu}_{J, \delta_i, \delta_j} = [\mu_J, \mu_\delta]^T, \quad (48)$$

and the covariance matrix becomes

$$\mathbf{V}_{J, \bar{\delta}} = \mathbf{A}_1 \cdot \mathbf{V}_{J, \delta_i, \delta_j} \cdot \mathbf{A}_1^T = \begin{bmatrix} \sigma_J^2 & r_{J, \delta} \sigma_J \sigma_\delta \\ r_{J, \delta} \sigma_J \sigma_\delta & \sigma_\delta^2 \frac{(1 + r_{\delta_i, \delta_j})}{2} \end{bmatrix}, \quad (49)$$

with the correlation coefficient

$$r_{J, \bar{\delta}} = \frac{r_{J, \delta} \sqrt{2}}{\sqrt{1 + r_{\delta_i, \delta_j}}}. \quad (50)$$

To obtain the Si-O-Si angle distribution,  $p(\Omega_0)$ , we continue with the following transformations

$$\text{Series B: } p(J, \bar{\delta}) \xrightarrow{B1} p(J, \langle \bar{\Omega} \rangle) \xrightarrow{B2} p(\Omega_0, \langle \bar{\Omega} \rangle).$$

*Step B1:* We transform  $p(J, \bar{\delta})$  to  $p(J, \langle \bar{\Omega} \rangle)$  using Eq. (40). In matrix notation this linear coordinate transformation is represented as

$$\begin{bmatrix} J \\ \langle \bar{\Omega} \rangle \end{bmatrix} = \underbrace{\begin{bmatrix} 1 & 0 \\ 0 & \frac{1}{a_\delta} \end{bmatrix}}_{\mathbf{A}_2} \begin{bmatrix} J \\ \bar{\delta} \end{bmatrix} + \underbrace{\begin{bmatrix} 0 \\ -\frac{b_\delta}{a_\delta} \end{bmatrix}}_{\mathbf{b}_2}. \quad (51)$$

Here  $\mathbf{A}_2$  is the affine transformation matrix and  $\mathbf{b}_2$  is a constant vector. The mean vector of the  $p(J, \langle \bar{\Omega} \rangle)$  distribution follows as

$$\boldsymbol{\mu}_{J, \langle \bar{\Omega} \rangle} = \mathbf{A}_2 \cdot \boldsymbol{\mu}_{J, \bar{\delta}} = \left[ \mu_J, \frac{\mu_\delta - b_\delta}{a_\delta} \right]^T, \quad (52)$$

and the covariance matrix becomes

$$\mathbf{V}_{J, \langle \bar{\Omega} \rangle} = \mathbf{A}_2 \cdot \mathbf{V}_{J, \bar{\delta}} \cdot \mathbf{A}_2^T = \begin{bmatrix} \sigma_J^2 & r_{J, \delta} \sigma_J \frac{\sigma_\delta}{a_\delta} \\ r_{J, \delta} \sigma_J \frac{\sigma_\delta}{a_\delta} & \frac{\sigma_\delta^2}{a_\delta^2} \frac{(1 + r_{\delta_i, \delta_j})}{2} \end{bmatrix}. \quad (53)$$



*Step B2:* The final transformation from  $p\left(J, \langle\overline{\Omega}\rangle\right)$  to  $p\left(\Omega_0, \langle\overline{\Omega}\rangle\right)$  distribution is performed numerically using the non-linear transformation in Eq. (38). For this we first construct the two dimensional probability distribution  $p\left(J, \langle\overline{\Omega}\rangle\right)$  from  $\boldsymbol{\mu}_{J, \langle\overline{\Omega}\rangle}$  and  $\mathbf{V}_{J, \langle\overline{\Omega}\rangle}$  following

$$p\left(J, \langle\overline{\Omega}\rangle\right) = \frac{\exp\left\{-\frac{1}{2}\left(\mathbf{x} - \boldsymbol{\mu}_{J, \langle\overline{\Omega}\rangle}\right)^T \cdot \left[\mathbf{V}_{J, \langle\overline{\Omega}\rangle}\right]^{-1} \cdot \left(\mathbf{x} - \boldsymbol{\mu}_{J, \langle\overline{\Omega}\rangle}\right)\right\}}{2\pi\sqrt{\det\left(\mathbf{V}_{J, \langle\overline{\Omega}\rangle}\right)}}, \quad (54)$$

where  $\mathbf{x} = \left[J, \langle\overline{\Omega}\rangle\right]^T$  and ‘det’ denotes matrix determinant. From the  $p\left(J, \langle\overline{\Omega}\rangle\right)$  distribution, we determine the  $p\left(\Omega_0, \langle\overline{\Omega}\rangle\right)$  distribution following

$$p\left(\Omega_0, \langle\overline{\Omega}\rangle\right) = \int_J p\left(J, \langle\overline{\Omega}\rangle\right) D\left[\Omega_0 - \Omega_0\left(J, \langle\overline{\Omega}\rangle\right)\right] dJ, \quad (55)$$

where the function  $D[\cdot]$  denotes the Dirac delta function and function  $\Omega_0(\cdot)$  is given by Eq. (38).

In principle, this entire mapping only requires the introduction of one additional parameter,  $r_{\delta_i, \delta_j}$ , the correlation coefficient between the isotropic chemical shift distributions, while the other statistical parameters characterizing  $p(J, \delta)$ , are determined from the experimental spectrum and given in Table II. Performing this analysis of the experimental results with just these assumptions, however, results in the statistics of

$$p(\Omega_0) = \int p\left(\Omega_0, \langle\overline{\Omega}\rangle\right) d\langle\overline{\Omega}\rangle, \quad (56)$$

not being consistent with

$$p\left(\langle\overline{\Omega}\rangle\right) = \int p\left(\Omega_0, \langle\overline{\Omega}\rangle\right) d\Omega_0, \quad (57)$$

for any value of  $r_{\delta_i, \delta_j}$ . To highlight this point we take  $r_{\delta_i, \delta_j} = 0.25$  which corresponds to  $r = r' = 0$  and obtain  $\mu_\Omega = 146.8^\circ$  and  $\mu_{\langle\overline{\Omega}\rangle} = 146.8^\circ$ , and  $\sigma_\Omega = 10.64^\circ$  and  $\sigma_{\langle\overline{\Omega}\rangle} = 8.0^\circ$  from the analysis of the experimental spectrum. While the two means are consistent, the two standard deviations are not. This can be seen by calculating the expected double mean standard deviation using Eq. (45) with  $r = r' = 0$  where one obtains

$$\sigma_{\langle\overline{\Omega}\rangle} = \sqrt{\frac{5}{32}}\sigma_\Omega. \quad (58)$$

Thus, if the standard deviation of  $p\left(\langle\overline{\Omega}\rangle\right)$  from the experimental 2D spectrum analysis has a standard deviation of  $\sigma_{\langle\overline{\Omega}\rangle} = 8.0^\circ$  then one would expect the standard deviation of  $p(\Omega_0)$

to be  $\sigma_\Omega = 20.2^\circ$ , a value that is significantly larger than the expected value of  $\sigma_\Omega = 10.64^\circ$ . This statistical inconsistency remains no matter what values of  $r$  and  $r'$  are investigated.

We believe the series of transformations given here are conceptually correct and that the source of the statistical inconsistency is the use of an incomplete relationship for  $^{29}\text{Si}$  isotropic chemical shift to local structure around  $\text{Q}^4$ . Specifically, there is a less established additional dependence on mean Si–O distance, which is commonly overlooked but noticed in porous siliceous zeolites by Lewis et. al<sup>61</sup>. They report an improved relationship between  $^{29}\text{Si}$  isotropic chemical shift and the local  $\text{Q}^4$  structure given by

$$\delta = b'_\delta + \frac{a'_\delta}{4} \sum_k \left( \langle d_{\text{Si-O},k} \rangle \frac{\cos \Omega_k}{\cos \Omega_k - 1} \right), \quad (59)$$

where  $\langle d_{\text{Si-O},k} \rangle$  is the mean Si–O bond distance of Si–O–Si linkage with angle  $\Omega_k$ . The summation over index  $k$  denotes all four Si–O–Si bond angles of the  $\text{Q}^4$ . The values  $a'_\delta = -216.95 \text{ ppm}/\text{\AA}$  and  $b'_\delta = 48.54 \text{ ppm}$  were obtained by Lewis et. al<sup>61</sup> after calibrating with respect to high silica zeolites ZSM-5(RT), ZSM-5(HT), Ferrierite(RT), Ferrierite(HT) where RT=room temperature, HT=high temperature, and the dense phase  $\text{SiO}_2$  polymorphs, Quartz and Cristobalite. The reason why this relationship is often overlooked, and that the previous relationships between chemical shift and mean Si–O–Si angle alone has applied so well in crystalline silicates, is due to the co-existence of a strong correlation between Si–O distance and Si–O–Si angle<sup>62,63</sup>. A similar issue arose in early efforts to determine the relationship between the  $^{17}\text{O}$  quadrupolar coupling constant and the Si–O–Si angle in silicates. In those studies the influence of the Si–O distance was included only through its parametric dependence on the Si–O–Si angle which was conventionally thought to vary according to a negative correlation discovered in crystalline silica polymorphs and further supported by potential energy surfaces determined in ab initio studies of small silicate clusters<sup>62,63</sup>. Instead of assuming this correlation Clark et al<sup>27</sup> determined a relationship for the  $^{17}\text{O}$  quadrupolar coupling constant that explicitly includes both Si–O distance and Si–O–Si angle and calibrated this expression with experimental  $^{17}\text{O}$  results from crystalline silica polymorphs, Coesite,  $\alpha$ -Quartz, Cristobalite, and Ferrierite(RT). Armed with this relationship Clark and others<sup>28,29</sup> discovered a counter-intuitive result from the  $^{17}\text{O}$  DAS spectrum of silica glass showing a positive correlation between Si–O distance and Si–O–Si angle. Thus, to proceed in our analysis we assume a line of regression in the correlation

between  $\langle d_{\text{Si-O},k} \rangle$  and  $\Omega_k$  in silica glass of the form

$$\langle d_{\text{Si-O},k} \rangle = d_{\text{Si-O}}^{\circ} + m_{\Omega}(\Omega_k - \Omega^*), \quad (60)$$

where  $\Omega^* = 150^\circ$ . As shown in appendix, one can invoke Eq. (60) and linearize Eq. (59) about  $\Omega^* = 150^\circ$  as

$$\delta = \underbrace{[\Lambda_0 d_{\text{Si-O}}^{\circ} + \Lambda_1 m_{\Omega}]}_{a_{\delta}} \langle \Omega \rangle + \underbrace{[b'_{\delta} + \Lambda_2 d_{\text{Si-O}}^{\circ} + m_{\Omega} \Lambda_3]}_{b_{\delta}}. \quad (61)$$

Equation (61) shows how the slope and intercept of the linear relationship between  $^{29}\text{Si}$  isotropic chemical shift and mean angle  $\langle \Omega \rangle$  depends on the trend between the Si-O-Si bond angle,  $\Omega$  and mean Si-O distance  $\langle d_{\text{Si-O}} \rangle$ . where  $\Lambda_0 = -0.543716 \text{ ppm}/(\circ \cdot \text{\AA})$ ,  $\Lambda_1 = -100.687 \text{ ppm}/\text{\AA}$ ,  $\Lambda_2 = -19.1295 \text{ ppm}/\text{\AA}$ , and  $\Lambda_3 = 15,103.03 \text{ ppm} \cdot \circ / \text{\AA}$ . In other words, we assume that the  $^{29}\text{Si}$  isotropic chemical shift relationship to mean angle has the same function form of Eq. (39) but now with an unknown  $a_{\delta}$  and  $b_{\delta}$  values which depend on the linear trend in the correlation between  $\langle d_{\text{Si-O},k} \rangle$  and  $\Omega_k$ .

Alternatively, one might also call into question the validity of Eq. (38) to account for the statistical inconsistency. Previous investigations of Eq. (38), however, were fairly exhaustive in determining  $^2J_{\text{Si-O-Si}}$  behavior in a wide range of cluster geometries—investigating dependences on Si-O distance, the central Si-O-Si linkage angle, the dihedral angle, and the outer Si-O-Si linkage angles. Thus, we are confident in its accuracy and robustness for interpreting  $^2J$  in both crystalline and glassy materials, regardless of the angle-distance correlation.

Since both  $^2J_{\text{Si-O-Si}}$  and  $\bar{\delta}$  depend on the same seven Si-O-Si angles associated with the  $\text{Q}_i^4\text{-Q}_j^4$  linkage we can propose a statistical model that provides the necessary constraints to keep  $p(\Omega_0)$  and  $p(\overline{\langle \Omega \rangle})$  statistically consistent and, at the same time, calibrate the unknown  $a_{\delta}$  and  $b_{\delta}$  values of Eq. (61). We begin by writing the covariance matrix derived from the analysis of the experimental spectrum as

$$\mathbf{V}_{\Omega_0, \langle \Omega \rangle}^{\{\text{exp}\}} = \begin{bmatrix} \sigma_{\Omega \text{exp}}^2 & \text{cov}(\Omega_0, \overline{\langle \Omega \rangle})_{\text{exp}} \\ \text{cov}(\Omega_0, \overline{\langle \Omega \rangle})_{\text{exp}} & \frac{\sigma_{\delta}^2 (1 + r_{\delta_i, \delta_j})}{2} \end{bmatrix}. \quad (62)$$

Because of the linear relationship of Eq. (40) or Eq. (61), the experimental variance of  $p(\overline{\langle \Omega \rangle})$  remains the same as in Eq. (53) through the numerical transformation of Eq. (55)—recalling that  $\sigma_{\delta}^2$  is obtained from the experimental isotropic chemical shift line shape. Taking

the mean and variance of  $p(\Omega_0)$  from experiment as the same as the model,

$$\mu_{\Omega_{\text{exp}}} = \mu_{\Omega}, \quad \text{and} \quad \sigma_{\Omega_{\text{exp}}}^2 = \sigma_{\Omega}^2, \quad (63)$$

we equate the covariance matrices of Eq. (62) and (45) and obtain the two constraints

$$\text{cov}(\Omega_0, \overline{\langle \Omega \rangle})_{\text{exp}} = \frac{\sigma_{\Omega}^2}{4}(3r + 1), \quad (64)$$

$$\frac{\sigma_{\delta}^2}{a_{\delta}^2} \frac{(1 + r_{\delta_i, \delta_j})}{2} = \frac{\sigma_{\Omega}^2}{32}(18r + 9r' + 5). \quad (65)$$

Substituting the expression of Eq. (43) for  $r_{\delta_i, \delta_j}$  into Eq. (65) leads to the solution

$$r = \frac{4}{3} \left( \frac{\sigma_{\delta}}{a_{\delta} \sigma_{\Omega}} \right)^2 - \frac{1}{3}. \quad (66)$$

Note, there is also an unphysical solution,  $r = -(5 + 9r')/18$ , which lies outside the bounds discussed below. For Eq. (66) and (64) to have a simultaneous solution in  $r$ , we substitute Eq. (66) in Eq. (64) and obtain

$$\boxed{\text{cov} \left( \Omega_0, \overline{\langle \Omega \rangle} \right)_{\text{exp}} = \frac{\sigma_{\Omega}^2}{4}(3r + 1) = \left( \frac{\sigma_{\delta}}{a_{\delta}} \right)^2}. \quad (67)$$

In Eq. (67) we have the constraints between the covariance of the experimentally derived distribution,  $p \left( \Omega_0, \overline{\langle \Omega \rangle} \right)$ , the model parameters,  $\sigma_{\Omega}$ ,  $r$ , and the slope  $a_{\delta}$ , all of which enforce statistical consistency.

Additionally, we find that the range of the correlation coefficients  $r$  and  $r'$  can be further constrained with this statistical model. In our analysis we combine the correlation coefficients  $r_{\langle \Omega \rangle_i, \langle \Omega \rangle_j}$ ,  $r_{\delta_i, \delta_j}$ ,  $r_{J, \delta}$  and  $r_{\Omega_0, \overline{\langle \Omega \rangle}}$  in Eqs. (43), (44), (50), and (46) respectively, with the experimentally determined correlation coefficient  $r_{J, \delta} = -0.5$  to determine the bounds on  $r \in \left[ -\frac{1}{3}, 1 \right]$  and a parametric dependence on  $r'$  as

$$r' \in \begin{cases} \left[ -1 - 4r, \frac{1}{3}(1 + 2r) \right] & r \in \left( -\frac{1}{3}, 0 \right] \\ \left[ \frac{1}{18}(36r^2 - 12r - 6), \frac{1}{3}(1 + 2r) \right] & r \in (0, 1] \end{cases} \quad (68)$$

This range of allowed values for  $r$  and  $r'$  are shown as the shaded area in Fig. 3. The associated  $r_{\delta_i, \delta_j}$  is indicated by the shaded contour colors with the corresponding legend on the right.

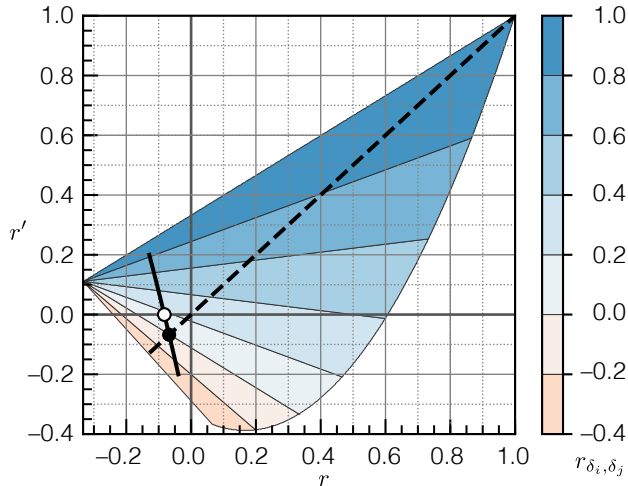


FIG. 3. Shaded area represents the statistically allowed correlation coefficients  $r$  and  $r'$ . The contour lines with corresponding legend on the right indicate the associated value of the correlation coefficient  $r_{\delta_i, \delta_j}$ . The dotted line corresponds to  $r = r'$ . The solid line represents the subset of  $r, r'$  values where a self consistent distribution is obtained from the analysis of experimental 2D spectrum. The closed and open circles represent the two solutions presented in Table IV.

To illustrate the statistical inconsistency when using the previous relationships between chemical shift and mean Si-O-Si angle alone, we take the slope,  $a_\delta = -0.6148$  ppm/ $^\circ$ , calibrated from crystalline silica polymorphs, and plot the three covariances of Eq. (67) in the case of  $r = 0$  in Fig 4A. Since solutions to Eq. (67) can only be true at the intersection of all three lines we clearly see that there can be no statistically consistent solution in this particular case.

To find solutions we adopt the iterative approach outlined in Algorithm 1. For each possible value of  $r'$  we apply this algorithm to determine the  $r$  value that satisfies Eq. (67). The results of this approach, giving all values of  $r$  and  $r'$  consistent with the experimental spectrum, are shown as the solid black line in Fig. 3. Not all of these solutions, however, are reasonable since a high value of  $|r_{\delta_i, \delta_j}|$  would lead to a greater fraction of  $^{29}\text{Si}$ - $^{29}\text{Si}$  pairs being in the strong  $J$  coupling limit. The more likely solutions are in the range near smaller values of  $|r_{\delta_i, \delta_j}|$ , and, as we will see, result in distribution statistics that are not significantly different. For example, in the case where  $r' = 0$  there is a single solution, shown as the open circle in Fig. 3, with  $r = -0.082$ ,  $a_\delta = -1.33$  ppm/ $^\circ$ , and  $b_\delta = \mu_\delta - a_\delta \mu_\Omega = 87.34$  ppm. Here

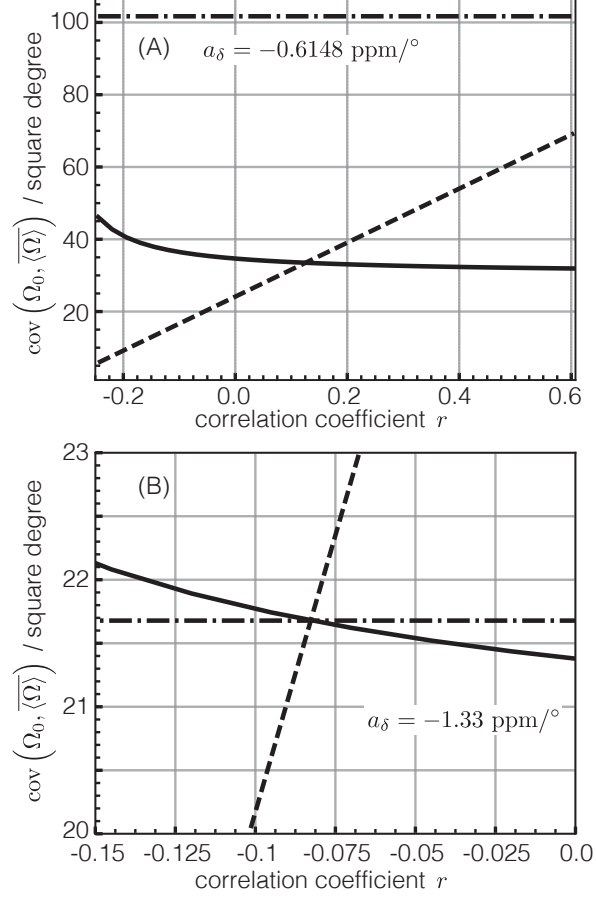


FIG. 4. Comparison of covariance  $\text{cov}(\Omega_0, \overline{\Omega})_{\text{exp}}$  (solid line), parametric dependence on  $r$  (dashed line) and  $(\sigma_\delta/a_\delta)^2$  (dot-dashed line) when  $r' = 0$  where  $r \in [-0.25, 0.608]$ . In (A)  $a_\delta = -0.6148 \text{ ppm}/^\circ$  and (B)  $a_\delta = -1.33 \text{ ppm}/^\circ$ . In (A), there is no point in  $r$  where a self consistent  $p(\Omega_0, \overline{\Omega})$  distribution is obtained.

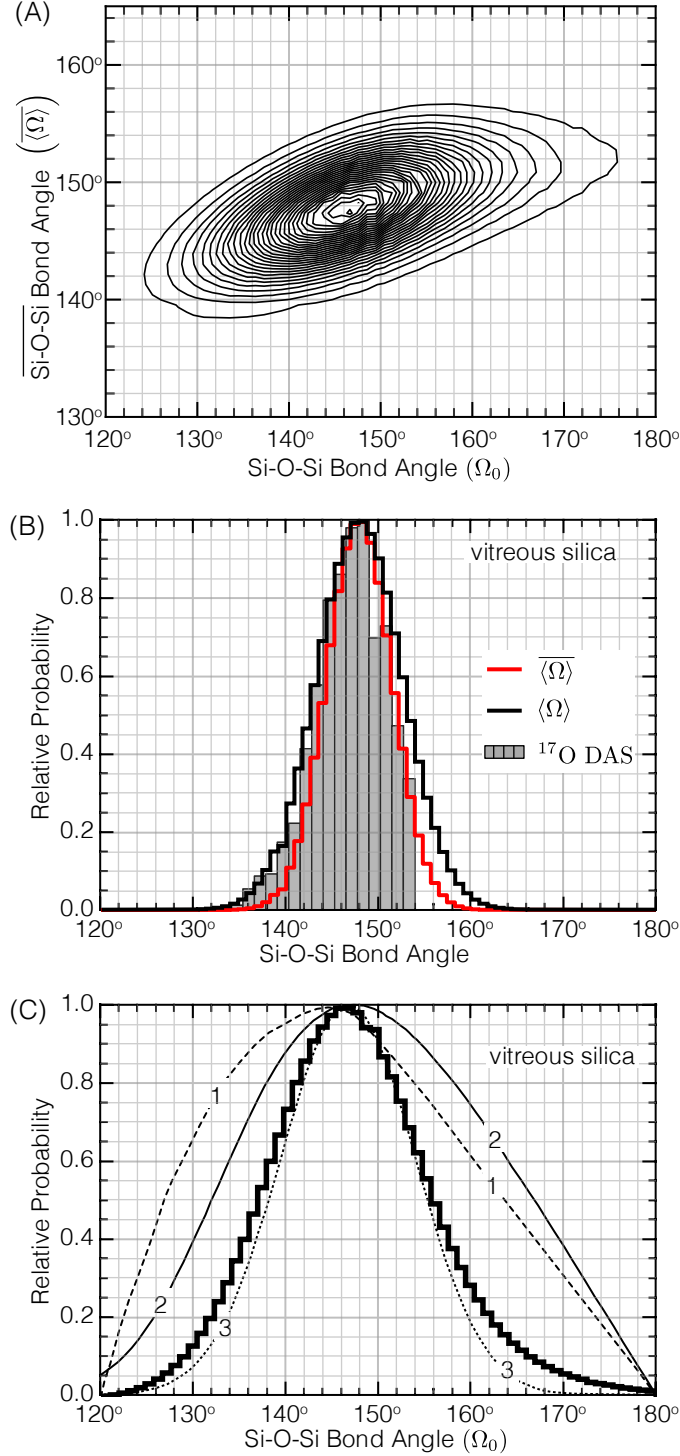


FIG. 5. (A) Correlation between Si-O-Si bond angle  $\Omega_0$  and double average angle  $\overline{\langle \Omega \rangle}$  when  $r' = 0$ . (B) Comparison of double average Si-O-Si bond angle distributions  $\overline{\langle \Omega \rangle}$  against Si-O-Si bond angle distributions from  $^{17}\text{O}$  DAS<sup>28</sup>. (C) Comparison of Si-O-Si bond angle distributions from various models. Line 1 XRD Mozzi and Warren model<sup>64</sup>, line 2, HXRD short range order (SRO) model<sup>65</sup>; line 3 HXRD/ND Neufeind and Liss chain<sup>66</sup> model. The bond angle distribution from current work is represented in bold line.

---

**Algorithm 1:** Iterative algorithm used in this analysis. The convergence is obtained when the absolute tolerance between the three covariances in Eq. (67) is less than  $0.005^\circ$ .

---

**input:**  $a_\delta, b_\delta, a_J, b_J, c_J, d_J, m_1, J_0$  (values from Table III);

**assign:**  $r, r'$ ;

**repeat**

Evaluate $r_{\delta_i, \delta_j}$ ;	/* Eq. (43) */
Evaluate $\mathbf{V}_{J, \langle \Omega \rangle}$ ;	/* Eq. (53) */
Construct $p\left(J, \langle \Omega \rangle\right)$ ;	/* Eq. (54) */
Compute $p\left(\Omega_0, \langle \Omega \rangle\right)$ ;	/* Eq. (55) */
Evaluate $\mu_\Omega, \sigma_\Omega^2, \sigma_{\langle \Omega \rangle}^2, \text{cov}\left(\Omega_0, \langle \Omega \rangle\right)_{\text{exp}}$ ;	
Update $r = \frac{4}{3} \left( \frac{\sigma_\delta}{a_\delta \sigma_\Omega} \right)^2 - \frac{1}{3}$ ;	/* Eq. (66) */
Update $a_\delta = -\frac{\sigma_\delta}{\sqrt{\text{cov}\left(\Omega_0, \langle \Omega \rangle\right)_{\text{exp}}}}$ ;	/* Eq. (67) */
Update $b_\delta = \mu_\delta - a_\delta \mu_\Omega$ ;	/* pivot at $(\mu_\delta, \mu_\Omega)$ */

**until** convergence;

**end**

---

$b_\delta$  is determined through the constraint of the mean of  $p(\Omega_0)$  and  $p(\langle \Omega \rangle)$  distributions being identical. This solution is illustrated as the intersection of the three lines in Fig. 4B where Eq. (67) is satisfied. This case corresponds to the physical situation where the Si-O-Si angle distributions which do not share a Si are entirely uncorrelated, i.e.,  $r' = 0$ . The resulting distribution  $p(\Omega_0, \langle \Omega \rangle)$  is presented in Fig. 5A. The projection onto the  $\Omega_0$  dimension in Fig. 5A gives  $p(\Omega_0)$ , the Si-O-Si bond angle distribution in silica glass presented as a bold solid line in Fig. 5C. The statistics of this distribution are given in Table IV. We also present the statistics in Table IV for the consistent solution with  $r = r'$  where there is a single solution, shown as the filled circle in Fig. 3, with  $r = r' = -0.068$ ,  $a_\delta = -1.3 \text{ ppm}/^\circ$ , and  $b_\delta = 82.54 \text{ ppm}$ . Comparing the two cases in Table IV illustrates the small degree of variation in the parameters along this solid line of solutions.



	$r' = r$	$r' = 0$
statistic	response	response
$\mu_{\Omega} = \mu_{\langle\Omega\rangle} = \mu_{\overline{\langle\Omega\rangle}}$	147.8°	147.8°
$\sigma_{\Omega}$	10.7°	10.7°
$\sigma_{\langle\Omega\rangle}$	4.8°	4.7°
$\sigma_{\overline{\langle\Omega\rangle}}$	3.4°	3.5°
$r$	-0.068	-0.082
$r_{\delta_i, \delta_j} = r_{\langle\Omega\rangle_i, \langle\Omega\rangle_j}$	-0.005	0.17
$r_{\Omega, \langle\Omega\rangle}$	0.45	0.43
$r_{\Omega, \overline{\langle\Omega\rangle}}$	0.63	0.57
mode	$\approx 147^\circ$	$\approx 147^\circ$
$a_{\delta}$	-1.3 ppm/°	-1.33 ppm/°
$b_{\delta}$	82.54 ppm	87.34 ppm

TABLE IV. Mean, Mode, standard deviations of Si-O-Si bond angle distributions and correlation coefficients between them for the two models  $r' = r$  (left) and  $r' = 0$  (right).

Distribution	Method	Bond angle distribution			
		$\mu_{\Omega}$	Mode	$\sigma_{\Omega}$	$\approx$ FWHM
Mozzi and Warren <sup>64</sup> (1969)	X-ray	147.9° <sup>53</sup>	144°	12.7°	37°
Neuefeind and Liss <sup>66</sup> (1996)	High energy X-ray	146.7°	146.8	7.3°	17°
Mauri et. al. <sup>53</sup> (2000)	<sup>29</sup> Si MAS NMR	151.4°	148°	11.3°	30°
Clark et. al. <sup>28</sup> (2004)	<sup>17</sup> O DAS NMR	146.6°	147°	3.8°	10°
Charpentier et. al. <sup>11</sup> (2009)	<sup>17</sup> O DAS NMR re-analysed	147.1°	147°	11.17°	23°
Charpentier et. al. <sup>11</sup> (2009)	<sup>29</sup> Si NMR	148.4°		10.8°	23°
This work	<sup>29</sup> Si-O- <sup>29</sup> Si $J$ -coupling NMR	147.8°	147°	10.7°	19°

TABLE V. Comparison of the mean, mode, and standard deviation of the Si-O-Si bond angle distribution in silica glass obtained from other experimental methods.

#### IV. RESULTS AND DISCUSSION

A contour plot of the self-consistent bi-variate probability distribution correlating the central Si-O-Si angle of a Q<sup>4</sup>-Q<sup>4</sup> linkage to its double mean Si-O-Si angle (seven angles) is given in Fig. 5A. In Figs. 5B and 5C are the 1D projections onto dimensions associated with the double mean Si-O-Si angle and central linkage angle, respectively. The statistics of the bi-variate distribution are given in Table IV. Although there is a strong correlation of  $r_{\Omega, \overline{\Omega}} = 0.57$  between these two distributions, this is expected as the central linkage angle is used in defining the double mean of Eq. (36). More noteworthy, however, is the relatively low value of the correlation coefficient,  $r = -0.082$ , for the four Si-O-Si angles of each Q<sup>4</sup> unit, determined with the underlying model of a septa-variate probability distribution of Si-O-Si angles in the Q<sup>4</sup>-Q<sup>4</sup> linkage (see Eq. (69)). The Si-O-Si angles in silica glass have been commonly assumed as uncorrelated in both diffraction<sup>64-66</sup> and NMR<sup>9,10,53,67,68</sup> analyses, although Malfait et al.<sup>69</sup> had argued against this assumption due to ring topology constraints. Here we find experimental confirmation of uncorrelated tetrahedral linkage angles in silica glass.

The 1D Si-O-Si bond angle distribution in silica glass derived from this bi-variable distribution (Fig. 5C) has a mean at 147.8°, a mode at 147° and a standard deviation of 10.7°. As mentioned earlier, some intensity at the larger Si-O-Si angles may be lost due to the non-weak couplings which corresponds to  $\sim 11.1\%$  of the total coupled resonances. A selected comparison of bond angle distribution statistics from silica glass obtained from other methods is shown in Table V. The often cited Si-O-Si bond angle distribution of Mozzi and Warren<sup>64</sup> for silica glass is also shown in Fig. 5C as line 1. While the mode of 144° falls close to our <sup>29</sup>Si <sup>2</sup>J-derived distribution, the width of Mozzi and Warren distribution is significantly wider—an observation that has generally been attributed to incorrect assumptions of uncorrelated angles and distances in Mozzi and Warren’s analysis<sup>1,66</sup>. Using assumptions nearly identical to Mozzi and Warren, Poulsen et al.<sup>65</sup> used high-energy X-rays measurements of silica glass to obtain the distribution shown as line 2 in Fig. 5C. Neuefeind and Liss<sup>66</sup> obtained the distribution shown as line 3 in Fig. 5C after reanalyzing high-energy X-ray<sup>70</sup> and neutron<sup>71,72</sup> diffraction data of silica glass. They attribute the narrowness of their distribution to a non-uniform distribution of dihedral angles, Si-O-Si-O, but find no evidence of correlation among Si-O distances, Si-O-Si angles, and the dihedral angles. This distribution

gives the closest agreement with our  $^{29}\text{Si}$  2D  $J$ -resolved spectrum-derived distribution.

An extensive comparison of experimental and MD predicted 1D Si-O-Si bond angle distributions in silica glass was given by Malfait et al.<sup>69</sup> in 2008. Overall, there is little agreement among the 1D Si-O-Si bond angle distributions obtained from various MD approaches, and no particular MD approach seems to give consistent agreement with the experimental values obtained here. Unfortunately, the possibility of a full-blown ab initio molecular dynamics (MD) simulation of a liquid cooled from the melt into the glassy state is decades away—maybe longer—from our current capabilities. The challenges to classical MD simulations today not only depend on finding accurate potentials but also in obtaining the computational resources to simulate the glass transition at a realistic cooling rate with a realistic number of atoms. Ab initio MD methods<sup>73</sup> have advanced significantly in the last decade and hold great promise, particularly in providing accurate potentials; however, it comes at the cost of even greater demands for computational resources which have yet to be realized.

In 2004, Clark et al.<sup>28</sup> measured and analyzed the  $^{17}\text{O}$  DAS spectrum of silica to obtain an angle distribution that agrees with the mean and mode obtained from our  $^{29}\text{Si}$  2D  $J$ -resolved spectral analysis but is considerably narrower in width. As described earlier<sup>29</sup>, however, the narrow width from the  $^{17}\text{O}$  DAS analysis is an artifact of an over-simplified assumption that each  $\omega_1$  (anisotropic) DAS spectrum cross-section contains a single site. In reality each  $\omega_1$  cross-section contains overlapping line shapes arising from a multitude of sites with varying  $C_q$ ,  $\eta_q$ , and  $^{17}\text{O}$  chemical shift. By modeling each cross section with a single site their analysis determines the mean  $C_q$  and  $\eta_q$  of each cross section. This biased the overall  $C_q$  and  $\eta_q$  distributions obtained from the full 2D spectrum towards a mean  $C_q$  and  $\eta_q$  distribution with smaller widths. Therefore, the previous  $^{17}\text{O}$  DAS results on silica<sup>28,29</sup> were analyzed in terms of a mean Si-O-Si bond angle distribution, which, as seen in Fig. 5B, compares favorably to the  $\langle\Omega\rangle$  distribution obtained from the  $J$ -resolved spectrum. Thus, we expect the correlations and the modes of the distributions obtained with  $^{17}\text{O}$  DAS to be accurate. It should be noted that the  $^{17}\text{O}$  DAS spectra analysis could be improved to obtain the individual  $\Omega$  distribution. Such an approach would be highly worthwhile as  $^{17}\text{O}$  DAS spectra still provides the most direct measure of the correlation between the distributions of Si-O-Si bond angle and Si-O distance.

In 2009, Charpentier et al.<sup>11</sup> re-analysed the  $^{17}\text{O}$  DAS spectrum and employed a more realistic  $p(C_q, \eta_q)$  distribution for modeling the  $^{17}\text{O}$  DAS and obtained a Si-O-Si distribution

that is consistent with our result derived from the  $^{29}\text{Si}$  2D  $J$ -resolved spectrum. Charpentier claim no evidence for the positive correlation between Si-O bond distance and Si-O-Si bond angle reported by Clark et al<sup>28</sup>, although we would caution that Charpentier’s re-calibration of the  $C_q$  relationship to Si-O-Si and Si-O distance used only  $^{17}\text{O}$  NMR results from Quartz, Cristoballite, and Coesite, and did not include  $^{17}\text{O}$  results from any siliceous porous silicates which can have a distinctly different angle-distance correlation.

Finally, we focus on the need to modify the linear relationship between the  $Q^4$   $^{29}\text{Si}$  chemical shift and mean Si-O-Si angle to obtain a self-consistent bi-variate distribution from the 2D spectrum correlating  $^{29}\text{Si}$  chemical shift and  $^2J_{\text{Si-O-Si}}$ . As we show in section III F, using the linear relationship of Eq. (39), calibrated on crystalline silica polymorphs, to analyze the experimental  $^{29}\text{Si}$  MAS spectrum of silica glass leads to a standard deviation of  $\sigma_\Omega = 20.2^\circ$ , significantly larger than all values in Table V, including the distribution of Mozzi and Warren. As noted earlier, it is an often overlooked fact that the  $^{29}\text{Si}$  isotropic chemical shift of a  $Q^4$  is dependent on both mean Si-O-Si bond angle and mean Si-O distance. Equation (61) further illustrates how the coefficients  $a_\delta$  and  $b_\delta$  in Eq. (39) depend on the trend in the correlation between the mean Si-O bond distance and Si-O-Si bond angle given by Eq. (60). A plot of mean Si-O bond distance and Si-O-Si bond angle of various crystalline silica polymorphs is shown in Fig. 6A and illustrate the well known negative trend in this particular correlation. This trend approximately follows  $m_\Omega = -0.25 \text{ pm}/^\circ$ , also shown in Fig. 6A as the solid black line. It is this value of  $m_\Omega$  in Eq. (61) that leads to  $a_\delta = -0.62 \text{ ppm}/^\circ$  and  $b_\delta = -19.82 \text{ ppm}$ . Interestingly, a similar plot for Ferrierite, shown as the solid black symbols in Fig. 6A, illustrate a different correlation between mean Si-O-Si bond angle and mean Si-O distance, approximately following  $m_\Omega \approx 0 \text{ pm}/^\circ$ , and shown in Fig. 6A as the dotted line.

Turning this argument around, we interpret the values of  $a_\delta = -1.33 \text{ ppm}/^\circ$  and  $b_\delta = 87.34 \text{ ppm}$ , obtained from our self-consistent analysis of the 2D  $J$ -resolved spectrum, using Eq. (61) and find  $m_\Omega = 0.459 \text{ pm}/^\circ$  and  $d_{\text{Si-O}}^\circ = 1.596 \text{ \AA}$ . This positive trend is shown as the dashed black line in Fig. 6A and is nearly orthogonal to the trend from crystalline silica polymorphs. More impressive is the excellent agreement between the trend obtained in this study and that obtained by Trease et al<sup>29</sup> from  $^{17}\text{O}$  DAS measurements on an ambient pressure silica glass, shown together in Fig. 6B. Also shown in Fig. 6B are the results of Trease et al.<sup>29</sup> on two other silica glasses densified at 8 and 13.5 GPa. In the three silica

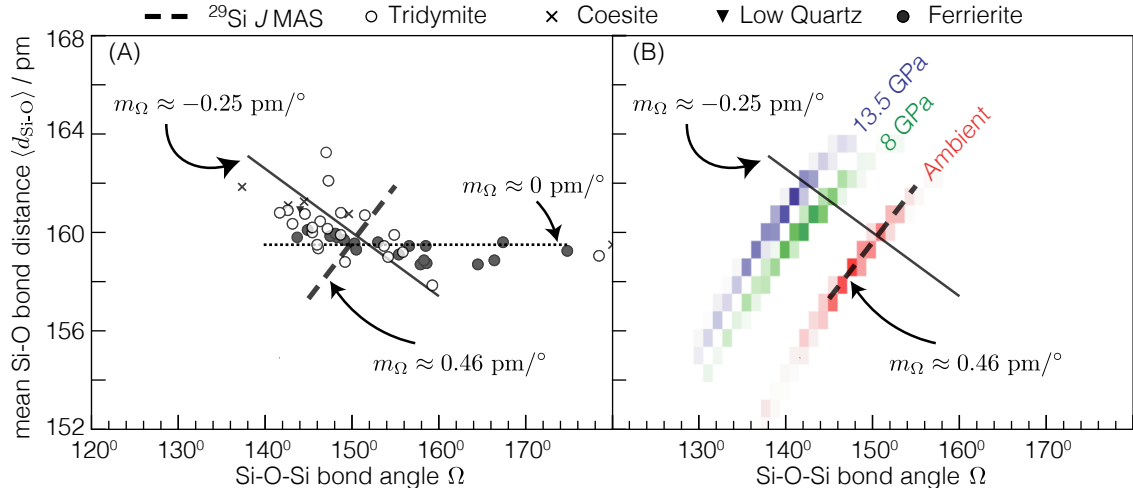


FIG. 6. (A) Correlation of Si-O bond distance and Si-O-Si bond angle for crystalline silica polymorphs along with the positive trend observed in silica glass (dashed black line). The negative angle-distance trend (solid black line) corresponding to  $m_{\Omega} = -0.25 \text{ pm}/^{\circ}$  is obtained from low Quartz, Coesite, and Tridymite. The solid black circles correspond to high silica Ferrierite structure with the negligible angle-distance trend shown in dotted line,  $m_{\Omega} \approx 0 \text{ pm}/^{\circ}$ . (B) Overlay of the 2D histogram correlating mean Si-O bond distance to mean Si-O-Si angle obtained by Trease et al.<sup>29</sup> on ambient and densified silica glasses along with the positive trend obtained from the analysis of the 2D  $J$ -resolved spectrum.

glasses of the Trease et al.<sup>29</sup> study and the ambient pressure silica glass of the Clark et al.<sup>28</sup> study a consistent positive trend in the correlation of Si-O-Si bond angle and Si-O distance is observed in agreement with the results of this study. Our analysis of the  $^{29}\text{Si}$  2D  $J$ -resolved spectrum provides an independent confirmation of this positive trend. Unlike the  $^{17}\text{O}$  DAS measurements, however, the strength of this positive correlation cannot be determined from the  $^{29}\text{Si}$  2D  $J$ -resolved measurement.

Given this growing evidence for a positive correlation between Si-O bond distance and Si-O-Si angle in silica glass, what is its physical origin? Clark et al.<sup>28</sup> invoked density fluctuations to explain the positive correlation between Si-O distance and Si-O-Si angle from their  $^{17}\text{O}$  DAS results of silica suggesting that smaller angles and distances correspond to higher density regions with smaller rings and vice versa. In this study, however, we find little to no correlation between Si-O-Si angles, i.e.,  $r \approx 0$ , that is, a result that would be

inconsistent with this hypothesis of density fluctuations. This positive correlation appears to be something more fundamental to the structure of silica glass and perhaps other fully connected tetrahedral networks. A more plausible explanation, recently proposed by Sen<sup>30</sup>, uses the concept of differential entropy to show that a positive correlation between angle and distance has a higher entropy than the negative correlation. And while a positive correlation between distributions is lower in entropy than fully uncorrelated distributions, Sen shows that the combination of entropic and energetic contributions stabilize the positive correlation in silica glass structure over both uncorrelated or negatively correlated distributions. Overall, this suggests that the notion that SiO<sub>4</sub> tetrahedra in silica glass are structurally identical to those in crystalline silica polymorphs is incorrect.

## V. SUMMARY

We have used the shifted-echo PIETA pulse sequence to measure the natural abundance <sup>29</sup>Si 2D *J*-resolved spectrum of silica glass. A full analysis of the NMR transition pathways in this experiment is given as well as a review of the effects of intermediate to strong couplings and the inter-echo delay times on the *J* modulated signal measured during echo train acquisition. By working with a <sup>29</sup>Si natural abundance sample we find that the doublets from isolated <sup>29</sup>Si-<sup>29</sup>Si pairs are dominant, making the 2D *J*-resolved spectrum of silica glass more easily analyzed than a <sup>29</sup>Si-enriched sample where multiplets are present. It is only through the sensitivity gain of PIETA that such a natural abundance strategy is possible.

Our analysis of the 2D *J*-resolved spectrum exploits a recently improved understanding<sup>32</sup> of the relationships between geminal *J* couplings and local structure of a Q<sup>4</sup>-Q<sup>4</sup> linkage in which knowledge of both <sup>2</sup>*J*<sub>Si-O-Si</sub> coupling and mean <sup>29</sup>Si chemical shift of a Q<sup>4</sup>-Q<sup>4</sup> linkage can be used to determine its central Si-O-Si linkage angle and the mean (seven) Si-O-Si linkage angle. Even then, this mapping of the 2D *J*-resolved spectrum of silica glass into the bi-variate distribution is not trivial, and requires additional assumptions that (1) the majority of the *J* couplings are in the weak limit, (2) there is a bivariate normal distribution of <sup>29</sup>Si chemical shifts of the two linked Q<sup>4</sup>, with a correlation coefficient determined in the mapping, and (3) the statistics of correlated angle distributions can be constrained with the assumption of a multi-variate (seven dimensional) normal distribution of angles in the Q<sup>4</sup>-Q<sup>4</sup> linkage. These three assumptions, however reasonable, do not lead to a statistically

consistent bi-variate probability distribution. Additional flexibility in the mapping must be introduced. This is done by assuming that a line of regression in the correlation between  $\langle d_{\text{Si-O}} \rangle$  and  $\Omega$  in silica glass, using an adjustable slope and intercept, can be combined with a known relationship<sup>61</sup> between isotropic  $^{29}\text{Si}$  chemical shift of a  $\text{Q}^4$  and its mean Si-O distance and mean Si-O-Si angle. This approach is suggested by the failure of previous attempts to determine the correct Si-O-Si angle distribution width from the  $^{29}\text{Si}$  MAS line shape. In other words, any relationship between  $^{29}\text{Si}$  chemical shift and mean Si-O-Si angle alone, when calibrated with  $^{29}\text{Si}$  chemical shifts of crystalline silicates, will be inappropriate for analyzing the  $^{29}\text{Si}$  MAS spectra of silica glass. Only with this added flexibility in the analysis can a statistically consistent bi-variate probability distribution correlating the central Si-O-Si angle to the mean Si-O-Si angle be obtained.

From our measurement and analysis of silica glass we determine that the Si-O-Si linkage angles are relatively uncorrelated and that the Si-O-Si angle distribution has a mean at  $147.8^\circ$ , a mode at  $147^\circ$  and a standard deviation of  $10.7^\circ$ . An unexpected outcome from our analysis is that the line of regression in the correlation between  $\langle d_{\text{Si-O}} \rangle$  and  $\Omega$  in silica needed to obtain this consistent bi-variate probability distribution reveals a positive correlation. This confirms a trend previously determined by  $^{17}\text{O}$  DAS measurements of ambient pressure and densified silica glasses, and recently interpreted as playing an important entropic role in determining the structure of a fully connected tetrahedral network of silica glass<sup>30</sup>.

## ACKNOWLEDGMENTS

This material is based upon work supported in part by the National Science Foundation under Grant No. CHE-1506870.

## VI. APPENDIX

### A. Statistical Model

Consider a seven dimensional multi-variate normal Si-O-Si bond angle distribution in silica glass about a  $\text{Q}^4$ - $\text{Q}^4$  linkage where individual bond angle distributions  $p(\Omega_k)$ 's are assumed to be identically described by a normal distribution with mean  $\mu_\Omega$  and standard deviation  $\sigma_\Omega$ . We represent the coordinate of this seven dimensional space by the vector

$\boldsymbol{\Omega} = [\Omega_3, \Omega_2, \Omega_1, \Omega_0, \Omega_4, \Omega_5, \Omega_6]$ . Furthermore, an individual bond angle distribution from this seven dimensional space is assumed to be identically correlated to another bond angle distribution with correlation coefficient  $r$  if the Si-O-Si bond angles share a Si. The other bond angle pairs are assumed to be correlated with a correlation coefficient  $r'$ . Under these assumptions we write the covariance matrix of  $p(\boldsymbol{\Omega})$  as

$$\mathbf{V}_7 = \sigma_{\Omega}^2 \begin{bmatrix} 1 & r & r & r & r' & r' & r' \\ r & 1 & r & r & r' & r' & r' \\ r & r & 1 & r & r' & r' & r' \\ r & r & r & 1 & r & r & r \\ r' & r' & r' & r & 1 & r & r \\ r' & r' & r' & r & r & 1 & r \\ r' & r' & r' & r & r & r & 1 \end{bmatrix}. \quad (69)$$

Exploiting the properties of linear transformations, we derive analytical expressions for the statistic of  $p(\Omega_0, \overline{\langle \Omega \rangle})$  distribution using the covariance matrix  $\mathbf{V}_7$ . We also derive expressions for the statistics of the  $p(\langle \Omega \rangle_i, \langle \Omega \rangle_j)$  and  $p(\delta_i, \delta_i)$  distributions.

1.  $p(\Omega_0, \overline{\langle \Omega \rangle})$  statistics

Following the definition of Eq. (36) the seven dimensional Si-O-Si bond angle distribution  $p(\boldsymbol{\Omega})$  is subjected to the following linear coordinate transformation

$$\begin{bmatrix} \Omega_0 \\ \overline{\langle \Omega \rangle} \end{bmatrix} = \frac{1}{8} \underbrace{\begin{bmatrix} 0 & 0 & 0 & 8 & 0 & 0 & 0 \\ 1 & 1 & 1 & 2 & 1 & 1 & 1 \end{bmatrix}}_{\mathbf{M}_1} \boldsymbol{\Omega}^T, \quad (70)$$

where  $\mathbf{M}_1$  is the coordinate transformation matrix. From  $\mathbf{M}_1$ , we derive the expression for the covariance matrix of  $p(\Omega_0, \overline{\langle \Omega \rangle})$  distribution,  $\mathbf{V}_{\Omega_0, \overline{\langle \Omega \rangle}} = \mathbf{M}_1 \cdot \mathbf{V}_7 \cdot \mathbf{M}_1^T$ , to obtain the expressions in Eqs. (45) and (46).



2.  $p(\langle\Omega\rangle_i, \langle\Omega\rangle_j)$  statistics

From the definition of Eq. (37) we construct a  $p(\langle\Omega\rangle_i, \langle\Omega\rangle_j)$  distribution by performing the following linear coordinate transformation

$$\begin{bmatrix} \langle\Omega\rangle_i \\ \langle\Omega\rangle_j \end{bmatrix} = \frac{1}{4} \underbrace{\begin{bmatrix} 1 & 1 & 1 & 1 & 0 & 0 & 0 \\ 0 & 0 & 0 & 1 & 1 & 1 & 1 \end{bmatrix}}_{\mathbf{M}_2} \boldsymbol{\Omega}^T, \quad (71)$$

where  $\mathbf{M}_2$  is the transformation matrix. From the covariance matrix for this distribution,  $\mathbf{V}_{\langle\Omega\rangle\langle\Omega\rangle} = \mathbf{M}_2 \cdot \mathbf{V}_7 \cdot \mathbf{M}_2^T$ , we obtain Eqs. (42) and (45).

3.  $p(\delta_i, \delta_j)$  statistics

Using the linear transformation

$$\delta_\lambda = a_\delta \langle\Omega\rangle_\lambda + b_\delta,$$

where  $\lambda = i$  or  $j$ , the distribution  $p(\langle\Omega\rangle_i, \langle\Omega\rangle_j)$  can be mapped to distribution  $p(\delta_i, \delta_j)$  when subjected to the following coordinate transformation

$$\begin{bmatrix} \delta_i \\ \delta_j \end{bmatrix} = \underbrace{\begin{bmatrix} a_\delta & 0 \\ 0 & a_\delta \end{bmatrix}}_{\mathbf{M}_3} \begin{bmatrix} \langle\Omega\rangle_i \\ \langle\Omega\rangle_j \end{bmatrix} + \underbrace{\begin{bmatrix} b_\delta \\ b_\delta \end{bmatrix}}_{\mathbf{b}_3}, \quad (72)$$

where  $\mathbf{M}_3$  is the affine transformation matrix and  $\mathbf{b}_3$  is a constant vector. The covariance matrix for  $p(\delta_i, \delta_j)$  distribution,  $\mathbf{V}_{\delta_i, \delta_j} = \mathbf{M}_3 \cdot \mathbf{V}_{\langle\Omega\rangle_i, \langle\Omega\rangle_j} \cdot \mathbf{M}_3^T$ , is given by

$$\mathbf{V}_{\delta_i, \delta_j} = a_\delta^2 \mathbf{V}_{\langle\Omega\rangle_i, \langle\Omega\rangle_j}, \quad (73)$$

and the correlation coefficient of Eq. (44) follows from  $\mathbf{V}_{\delta_i, \delta_j}$ .

**B.  $^{29}\text{Si}$  chemical shift dependence on Si-O distance**

To compare Eq. (59) with the linear relationship in Eq. (39), we consider a linear trend of Eq. (60). Substituting Eq. (60) in Eq. (59), followed by a linearization using a series expansion in  $\Omega_k$  about  $\Omega^*$  we have

$$\delta = (a'_\delta x_2 d_{\text{Si-O}}^0 + a'_\delta x_1 m_\Omega) \langle \Omega \rangle + (x_1 a'_\delta - x_2 a'_\delta \Omega^*) d_{\text{Si-O}}^0 - a'_\delta x_1 m_\Omega \Omega^* + b'_\delta \quad (74)$$

where  $x_1 = (2\sqrt{3} - 3)$  and  $x_2 = \frac{\pi}{90^\circ} (7 - 4\sqrt{3})$  are coefficients from the series expansion. Here  $\langle \Omega \rangle = \frac{1}{4} \sum_k \Omega_k$  is the average Si-O-Si bond angle about the Si tetrahedron. Expanding about  $\Omega^* = 150^\circ$  leads to

$$\begin{aligned} \Lambda_0 &= a'_\delta x_2 &= -0.543716 \text{ ppm}/(\text{^\circ} \cdot \text{\AA}), \\ \Lambda_1 &= a'_\delta x_1 &= -100.687 \text{ ppm}/\text{\AA}, \\ \Lambda_2 &= \Lambda_1 - \Lambda_0 \Omega^* &= -19.1295 \text{ ppm}/\text{\AA}, \\ \Lambda_3 &= -\Lambda_1 \Omega^* &= 15103.03 \text{ ppm}\cdot\text{^\circ}/\text{\AA}, \end{aligned} \quad (75)$$

and the expression in Eq. (74) reduces to Eq. (61). Equation (61) shows how the slope and intercept of the linear relationship of Eq. (39) between  $^{29}\text{Si}$  isotropic chemical shift and mean angle  $\langle \Omega \rangle$  depends on the trend between the Si-O-Si bond angle,  $\Omega$ , and the mean Si-O distance,  $\langle d_{\text{Si-O}} \rangle$ .

- <sup>1</sup> A. Wright, *J. Non Cryst. Solids* **179**, 84 (1994).
- <sup>2</sup> A. C. Hannon, “Neutron diffraction techniques for structural studies of glasses,” in *Modern Glass Characterization* (Wiley-Blackwell, 2015) Chap. 5, pp. 1–83.
- <sup>3</sup> P. Biswas, D. N. Tafen, F. Inam, B. Cai, and D. A. Drabold, *Journal of Physics: Condensed Matter* **21**, 084207 (2009).
- <sup>4</sup> R. L. McGreevy and L. Pusztai, *Molec. Sim.* **1**, 359 (1988).
- <sup>5</sup> R. L. McGreevy, *Journal of Physics Condensed Matter* **13**, R877 (2001).
- <sup>6</sup> A. Pandey, P. Biswas, and D. A. Drabold, *Scientific Reports* **6**, 33731 (2016).
- <sup>7</sup> D. A. Drabold, *Eur. Phys. J. B* **68**, 1–21 (2009).
- <sup>8</sup> M. Eden, *Annu. Rep. Prog. Chem., Sect. C: Phys. Chem.* **108**, 177 (2012).
- <sup>9</sup> E. Dupree and R. F. Pettifer, *Nature* **308**, 523 (1984).
- <sup>10</sup> L. F. Gladden, T. A. Carpenter, and S. R. Elliott, *Phil. Mag. B* **53**, L81 (1986).
- <sup>11</sup> T. Charpentier, P. Kroll, and F. Mauri, *J. Phys. Chem. C* **113**, 7917 (2009).
- <sup>12</sup> I. Farnan, P. J. Grandinetti, J. H. Baltisberger, J. F. Stebbins, U. Werner, M. A. Eastman, and A. Pines, *Nature* **358**, 31 (1992).

- <sup>13</sup> B. F. Chmelka, K. T. Mueller, A. Pines, J. F. Stebbins, Y. Wu, and J. W. Zwanziger, *Nature* **339**, 42 (1989).
- <sup>14</sup> K. T. Mueller, B. Q. Sun, G. C. Chingas, J. W. Zwanziger, T. Terao, and A. Pines, *J. Magn. Reson.* **86**, 470 (1990).
- <sup>15</sup> K. T. Mueller, Y. Wu, B. F. Chmelka, J. Stebbins, and A. Pines, *J. Am. Chem. Soc.* **113**, 32 (1991).
- <sup>16</sup> P. J. Grandinetti, J. H. Baltisberger, A. Llor, Y. K. Lee, U. Werner, M. A. Eastman, and A. Pines, *J. Magn. Reson. A* **103**, 72 (1993).
- <sup>17</sup> H. K. C. Timken, S. E. Schramm, R. J. Kirkpatrick, and E. Oldfield, *J. Phys. Chem.* **91**, 1054 (1987).
- <sup>18</sup> J. A. Tossell and P. Lazzeretti, *Chem. Phys. Lett.* **112**, 205 (1987).
- <sup>19</sup> J. A. Tossell and P. Lazzeretti, *Phys. Chem. Minerals* **15**, 564 (1988).
- <sup>20</sup> C. G. Lindsay and J. A. Tossell, *Phys. Chem. Minerals* **18**, 191 (1991).
- <sup>21</sup> P. J. Grandinetti, J. H. Baltisberger, U. Werner, A. Pines, I. Farnan, and J. F. Stebbins, *J. Phys. Chem.* **99**, 12341 (1995).
- <sup>22</sup> K. E. Vermillion, P. Florian, and P. J. Grandinetti, *J. Chem. Phys.* **108**, 7274 (1998).
- <sup>23</sup> T. M. Clark and P. J. Grandinetti, *Solid State NMR* **16**, 55 (2000).
- <sup>24</sup> T. M. Clark and P. J. Grandinetti, *J. Non-Cryst. Solids* **265**, 75 (2000).
- <sup>25</sup> T. M. Clark, P. J. Grandinetti, P. Florian, and J. F. Stebbins, *J. Phys. Chem. B* **105**, 12257 (2001).
- <sup>26</sup> T. M. Clark and P. J. Grandinetti, *Solid State NMR* **27**, 233 (2005).
- <sup>27</sup> T. M. Clark and P. J. Grandinetti, *J. Phys. Condensed Matter* **15**, S2387 (2003).
- <sup>28</sup> T. M. Clark, P. J. Grandinetti, P. Florian, and J. F. Stebbins, *Phys. Rev. B* **70**, 064202 (2004).
- <sup>29</sup> N. M. Trease, T. M. Clark, P. J. Grandinetti, J. F. Stebbins, and S. Sen, *J. Chem. Phys.* **146**, 184505 (2017).
- <sup>30</sup> S. Sen, *J. Non-Cryst. Solids* **486**, 9 (2018).
- <sup>31</sup> J. H. Baltisberger, B. J. Walder, E. G. Keeler, D. C. Kaseman, K. J. Sanders, and P. J. Grandinetti, *J. Chem. Phys.* **136**, 211104 (2012).
- <sup>32</sup> D. J. Srivastava, P. Florian, J. H. Baltisberger, and P. J. Grandinetti, *Physical Chemistry Chemical Physics* **20**, 562 (2018).
- <sup>33</sup> P. Florian, F. Fayon, and D. Massiot, *J. Phys. Chem. C* **113**, 2562 (2009).

- <sup>34</sup> M. M. Maricq and J. S. Waugh, *J. Chem. Phys.* **70**, 3300 (1979).
- <sup>35</sup> A. Allerhand, *J. Chem. Phys.* **44**, 1 (1966).
- <sup>36</sup> R. Freeman and H. D. W. Hill, *J. Chem. Phys.* **54**, 301 (1971).
- <sup>37</sup> P. J. Grandinetti, J. T. Ash, and N. M. Trease, *Prog. Nucl. Mag. Res. Sp.* **59**, 121 (2011).
- <sup>38</sup> G. Bodenhausen, H. Kogler, and R. R. Ernst, *J. Magn. Reson.* **58**, 370 (1984).
- <sup>39</sup> See Supplemental Material at [URL will be inserted by publisher] for additional theoretical details on the line shape model for the weak  $^2J_{\text{Si-O-Si}}$  couplings, the NMR pulse sequence, signal processing scripts, and the experimental NMR signal data.
- <sup>40</sup> J. A. Aguilar, M. Nilsson, G. Bodenhausen, and G. A. Morris, *Chem. Commun.* **48**, 811 (2012).
- <sup>41</sup> K. Takegoshi, K. Ogura, and K. Hikichi, *Journal of Magnetic Resonance (1969)* **84**, 611 (1989).
- <sup>42</sup> P. C. van Zijl, C. T. Moonen, and M. von Kienlin, *Journal of Magnetic Resonance (1969)* **89**, 28 (1990).
- <sup>43</sup> B. J. Walder, K. K. Dey, M. C. Davis, J. H. Baltisberger, and P. J. Grandinetti, *J. Chem. Phys.* **142**, 014201 (2015).
- <sup>44</sup> Details on how a  $\pi/2$  pulse splits each of the eight transition pathways above into 13 pathways, which are then reduced down to only 32 detectable transition pathways at  $t = 0$  through constructive and destructive interference of the labeled pairs of transition pathways in Eqs. (10) and (11) above are given in the Supplemental Material<sup>39</sup>.
- <sup>45</sup> R. H. Lamoreaux, D. L. Hildenbrand, and L. Brewer, *J. Phys. Chem. Ref. Data* **16**, 419 (1987).
- <sup>46</sup> Z. H. Gan, *J. Am. Chem. Soc.* **122**, 3242 (2000).
- <sup>47</sup> H. T. Kwak and Z. H. Gan, *J. Magn. Reson.* **164**, 369 (2003).
- <sup>48</sup> PhySy Ltd., “RMN 1.1,” (2017).
- <sup>49</sup> E. L. Hahn and D. E. Maxwell, *Phys. Rev.* **88**, 1070–1084 (1952).
- <sup>50</sup> L. Duma, W. C. Lai, M. Carravetta, L. Emsley, S. P. Brown, and M. H. Levitt, *Chem. Phys. Chem.* **5**, 815 (2004).
- <sup>51</sup> J. H. Baltisberger, P. Florian, E. G. Keeler, P. A. Phyto, K. J. Sanders, and P. J. Grandinetti, *J. Magn. Reson.* **268**, 95 (2016).
- <sup>52</sup> J. Mahler and A. Sebald, *Solid-State NMR* **5**, 63 (1995).
- <sup>53</sup> F. Mauri, A. Pasquarello, B. G. Pfrommer, Y.-G. Yoon, and S. G. Louie, *Phys. Rev. B* **62**, 4786 (2000).
- <sup>54</sup> A. Azzalini and A. Capitanio, The Skew-Normal and Related Families, Institute of Mathemat-

- ical Statistics Monographs (Cambridge University Press, Cambridge, UK, 2014).
- <sup>55</sup> J. R. Bodart, V. P. Bork, T. Cull, H. Ma, P. A. Fedders, D. J. Leopold, and R. E. Norberg, *Phys. Rev. B* **54**, 15291 (1996).
- <sup>56</sup> M. Newville, T. Stensitzki, D. B. Allen, and A. Ingargiola, “Lmfit: Non-linear least-square minimization and curve-fitting for python,” (2014).
- <sup>57</sup> S. van der Walt, S. C. Colbert, and G. Varoquaux, *Computing in Science & Engineering* **13**, 22 (2011).
- <sup>58</sup> J. D. Hunter, *Computing in Science & Engineering* **9**, 90 (2007).
- <sup>59</sup> J. V. Smith and C. S. Blackwell, *Nature* **303**, 223 (1983).
- <sup>60</sup> G. Engelhardt and R. Radeglia, *Chemical Physics Letters* **108**, 271 (1984).
- <sup>61</sup> J. R. Lewis, C. C. Freyhardt, and M. E. Davis, *J. Phys. Chem.* **100**, 5039 (1996).
- <sup>62</sup> G. V. Gibbs, *Am. Miner.* **67**, 421 (1982).
- <sup>63</sup> G. Gibbs, A. Wallace, D. Cox, R. Downs, N. Ross, and K. Rosso, *Am. Min.* **94**, 1085 (2009).
- <sup>64</sup> R. L. Mozzi and B. E. Warren, *J. Appl. Cryst.* **2**, 164 (1969).
- <sup>65</sup> H. Poulsen, J. Neufeind, H. Neumann, J. Schneider, and M. Zeidler, *Nuclear Instruments and Methods in Physics Research Section B: Beam Interactions with Materials and Atoms* **97**, 162 (1995).
- <sup>66</sup> J. Neufeind and K.-D. Liss, *Berichte der Bunsen-Gesellschaft-Phys. Chem. Chem. Phys.* **100**, 1341 (1996).
- <sup>67</sup> R. Oestrike, W. Yang, R. J. Kirkpatrick, R. L. Hervig, A. Navrotsky, and B. Montez, *Geochim. Cosmochim. Acta* **51**, 2199 (1987).
- <sup>68</sup> R. F. Pettifer, R. Dupree, I. Farnan, and U. Sternberg, *J. Non-Cryst. Solids* **106**, 408 (1988).
- <sup>69</sup> W. J. Malfait, W. E. Halter, and R. Verel, *Chemical Geology* **256**, 269 (2008).
- <sup>70</sup> H. Poulsen, J. Neufeind, H.-B. Neumann, J. Schneider, and M. Zeidler, *J. Non-Cryst. Solids* **188**, 63 (1995).
- <sup>71</sup> P. A. V. Johnson, A. Wright, and R. N. Sinclair, *J. Non Cryst. Solids* **58**, 109 (1983).
- <sup>72</sup> D. I. Grimley, A. Wright, and R. N. Sinclair, *J. Non Cryst. Solids* **119**, 49 (1990).
- <sup>73</sup> D. Marx and J. Hutter, *Ab Initio Molecular Dynamics: Basic Theory and Advanced Methods* (Cambridge University Press, Cambridge, 2009).